SECURITY CLASSIFICATION OF THIS PAGE (When Data Entered)

REPORT DOCUMENTATION PAGE

READ INSTRUCTIONS BEFORE COMPLETING FORM

1. REPORT NUMBER: 318-037-008
2. GOVT ACCESSION NO.
3. RECIPIENT'S CATALOG NUMBER

4. TITLE (and Subtitle): Acoustically Scanned Optical Imaging Devices, A074954
5. TYPE OF REPORT & PERIOD COVERED: Technical Report
6. PERFORMING ORG. REPORT NUMBER: GL-3089
7. AUTHOR(s): G. S. Kino, J. Bowers, B. Khuri-Yakub, R. Thornton
8. CONTRACT OR GRANT NUMBER(s): N00014-76-C-0129, ARPA Order-2778
9. PERFORMING ORGANIZATION NAME AND ADDRESS: Edward L. Ginzton Laboratory, W. W. Hansen Laboratories of Physics, Stanford University, Stanford, CA 94305
10. PROGRAM ELEMENT, PROJECT, TASK AREA & WORK UNIT NUMBERS: PE 61101E, 8D10, Order No. 2778-5
11. CONTROLLING OFFICE NAME AND ADDRESS: Defense Advanced Research Projects Agency, 1400 Wilson Boulevard, Arlington, VA 22209
12. REPORT DATE: February 1980
13. NUMBER OF PAGES: 79
14. MONITORING AGENCY NAME & ADDRESS (if different from Controlling Office): Office of Naval Research, Code 427, Arlington, VA 22217
15. SECURITY CLASS. (of this report): Unclassified
15a. DECLASSIFICATION/DOWNGRADING SCHEDULE

16. DISTRIBUTION STATEMENT (of this Report)

NR-318-737 Rev ONR

Approved for public release; distribution unlimited

17. DISTRIBUTION STATEMENT (of the abstract entered in Block 20, if different from Report)

Semiannual rept. no. 9, 1 Jul - 31 Dec 79

18. SUPPLEMENTARY NOTES

ONR Scientific Office
Tel: (202) 696-4218

19. KEY WORDS (Continue on reverse side if necessary and identify by block number)

Storage correlators; Acoustic surface waves; Schottky diodes; Zinc oxide; Matching; Adaptive filters

20. ABSTRACT (Continue on reverse side if necessary and identify by block number)

~~We have demonstrated~~ HAS BEEN DEMONSTRATED broadband ZnO on Si acoustic surface wave devices with a 40 MHz bandwidth. ~~We are~~ making use of a new highly flexible iterative technique for the design of broadband matching networks. ~~We have demonstrated~~ HAS ALSO BEEN DEMONSTRATED the first ZnO on Si Schottky diode correlator. Work proceeds on ZnO magnetron sputtering processes, with some problems due to badly oriented gold. These have been cured.

409646

DD FORM 1 JAN 73 1473 EDITION OF 1 NOV 65 IS OBSOLETE
S/N 0102-LF-014-6601

SECURITY CLASSIFICATION OF THIS PAGE (When Data Entered)

ACOUSTICALLY SCANNED OPTICAL IMAGING DEVICES

Semiannual Report No. 9

1 July - 31 December, 1979

Principal Investigator:

G. S. Kino
(415) 497-0205

Sponsored by
Advanced Research Projects Agency
ARPA Order No. 2778

Contract N00014-76-C-0129
Program Code Number: 4D10
Contract Period: 1 July - 31 December, 1979
Amount of Contract: $504,302.00
Form Approved, Budget Bureau - No. 22R0293

G. L. Report No. 3089

February 1980

Edward L. Ginzton Laboratory
W. W. Hansen Laboratories of Physics
Stanford University
Stanford, California

TABLE OF CONTENTS

I. MANAGEMENT REPORT

A. Summary

The major development in the last few months has been the demonstration of broadband, Sezawa mode ZnO devices. We have demonstrated devices with a 40 MHz bandwidth, i.e., approximately 25% . We have also developed an entirely new program for the design of matching networks to arbitrary loads. We believe that this is extremely important because it is not based on the usual matching network approach. Instead, it is based on the development of our adaptive filter concepts in which we postulate the form of the matching network, then adjust its parameters on the computer in a manner equivalent to trimming the elements to obtain the optimum broadband match. The technique is an iterative one which converges after a large number of iterations, but which has tremendous flexibility. Ultimately, it should be possible to design bulk and surface wave transducers, and the matching network as one package, adjusting all parameters for the optimum conditions, whether they be minimum loss, linear phase or some other parameter like good transient response, which is of interest to the designer. The technique basically minimizes the mean squared error between a desired response and the response obtained; so it has a great deal of flexibility.

We have demonstrated a monolithic Schottky diode devices for the first time. We have shown that we can indeed make Schottky diode correlators with turn-on times of the order of a few ns . We have also recently been examining the possibility of putting silicon on $LiNbO_3$ and laser annealing. In cooperation with Gibbons, we are intending to work toward an alternative Schottky diode device based on the silicon-lithium niobate configuration. We have new ideas for putting the diodes on the underside

of the silicon and we will be testing these systems along with ZnO on Schottky diode correlators in the next few months.

We have had some difficulties with the ZnO deposition because of problems with the Au layers. Unfortunately there was a change in the substrate holder and the method of mounting the substrate in the holder, which had not been checked out sufficiently carefully. Consequently, the thermal contact was poor and the gold layers that were being put down, which had been reproducible for several years, were now no longer properly oriented, and therefore led to poor ZnO . Consequently, most of our transducers had rather poor performance, even though the quality of the ZnO on the SiO_2 was excellent, and better than we had ever seen before. Unfortunately, our checks with a bulk wave transducer were not reliable because the bulk wave transducers worked well with the use of a different substrate holder. This difficulty has now been corrected and we should not have too many problems in the future.

B. Research Program Plan

We will continue to test ZnO deposition on a wide range of materials. We will carry out some laser annealing experiments. We will construct and test broadband ZnO on Si correlators and test out further ZnO on Si Schottky diode correlators.

C. Major Accomplishments

We have demonstrated a Schottky diode ZnO on Si correlator for the first time. We have arrived at entirely new techniques for designing broadband ZnO on Si devices with a demonstrated 40 MHz bandwidth. We expect to be able to obtain still larger bandwidths (60-70 MHz). Sezawa

mode devices and important new matching network design theories with broad-scale applications have been developed.

D. Problems Encountered

No major problems have been encountered.

E. Fiscal Status

Total amount of contract	$504,302
Expenditures & commitments through 12/31/79	$417,115
Estimated funds required to complete work	$87,187
Estimated date of completion of work	30 September 1980

F. Action Required by ARPA/ONR

No action required at the present time.

II. TECHNICAL PROGRESS REPORT

A. Sezawa Wave Devices and Theory

In the last report, theoretical values for phase velocity and coupling coefficient for (001) ZnO on (001) cut (100) prop. Si were presented. We have since made Sezawa wave delay lines and convolvers which exhibited the high coupling coefficient $\Delta v/v = .028$ which we theoretically predicted for (001) Si. We have also obtained experimental and theoretical results for (111) Si. The details of these results are presented in Appendix I, which is a preprint of a paper submitted to Applied Physics Letters. Only the highlights of this paper and some additional results will be presented in this section.

The goal of the present work on Sezawa waves was to demonstrate broadband thin film ZnO/Si devices, and this was achieved. Delay lines with 3 dB bandwidths of 31 MHz with 23 dB loss and 42 MHz with 35 dB loss were demonstrated. This compares very favorably with the best results for ZnO/Si Rayleigh wave devices: 18 MHz bandwidth with 22 dB loss[1] and 22 MHz bandwidth with 30 dB loss.[2]

Sezawa wave convolvers were also fabricated using (001) Si. These devices all had a high insertion loss due to a combination of two problems: poorly oriented ZnO under the transducers and interaction losses with the electrons in the central Si region. However, due to the high coupling coefficient in the center region, these devices had excellent internal convolution efficiency (-27 dBm). As a result of the high coupling coefficient in the center region, the insertion loss in these devices could be varied by 45 dB by adjusting the top plate bias. This is much

higher than the 1 to 3 dß variation seen in Rayleigh wave ZnO/Si devices,[3] and indicates that high gain Sezawa wave amplifiers could be made.

Theoretical values for coupling coefficient and phase velocity have been obtained for the Sezawa mode (second order Rayleigh mode) for ZnO on substrates of (001) Si, (111) Si, and for (001) $LiNbO_3$ on (001) Si. Theoretical values have also been obtained for the third order Rayleigh mode for ZnO on (001) Si. We have concluded that the use of (001) Si as a substrate is preferred for three reasons: (1) the highest coupling coefficient is obtained with this substrate; (2) the peak in the coupling coefficient occurs at a lower value of hk for this substrate, and hence it has the largest value of series capacitance, which makes tuning easier and allows broader bandwidth; and (3) since hk is smaller for (001) Si, this means thinner films can be used, and we expect fewer bulk wave problems. The use of ZnO on (111) Si is the next best choice, and because of the lower coupling coefficient and higher series capacitance, the electronic Q is twice as high as for (001) Si.

Optimum Matching Network

A question consistently encountered in all of our acoustics work has been to determine what is the maximum bandwidth attainable for a given loss if the ideal matching network were used. The answer to this question allows us to determine if our matching networks are close to ideal, and it would also allow us to compare the use of different materials and wave modes.

This question was first answered by Bode[4] for a parallel R-C combination, and later by Fano[5] for series R-L and several other slightly more complicated situations. Their results will be applied here, although

we expect that the maximum bandwidth attainable will be slightly less since the radiation resistance varies with frequency, and since we are neglecting pad capacity. The neglect of pad capacity is a good approximation for Sezawa wave IDTs and $LiNbO_3$ IDTs, but a poor approximation for ZnO/Si Rayleigh wave devices.

For an IDT, the minimum loss L for a given fractional bandwidth f for an ideal coupling network is

$$L = \frac{1}{1 - e^{-2\pi fQ}} \qquad (1)$$

where $Q = 1/\omega R_{ao} C_T$ and R_{ao} is the radiation resistance at center frequency and C_T is the transducer finger capacity. This relationship is shown in Fig. 1 for a number of interesting cases. It can be seen that ZnO/Si Sezawa wave IDTs and $LiNbO_3$ Rayleigh wave IDTs are essentially equivalent while conventional Rayleigh wave ZnO/Si devices have inherently much higher electronic mismatch loss.

These results indicate that 40 MHz bandwidths for our Sezawa wave IDTs are achievable with much lower insertion losses than we have observed. Consequently, we developed an optimization algorithm which will determine the optimum component values of an arbitrary matching network. This algorithm is described in the next section.

Optimization Algorithm

This algorithm is based on our earlier studies of adaptive filters. It finds the component values which minimize the mean square error between the desired frequency response and the actual frequency response

over a given frequency range. The number of components and the configuration of components must be specified by the user.

Consider a generalized network as shown in Fig. 2 where the transducer frequency response is $X(\omega)$ and the frequency response of the network and transducer is

$$Y(\omega) = H(\omega)\, X(\omega) \tag{2}$$

X and Y can be voltages, powers, or some other parameter of interest. If the desired frequency response is $D(\omega)$, then the error is

$$E(\omega) = D(\omega) - Y(\omega) = D - H(\omega)\, X(\omega) \tag{3}$$

Suppose that H is a function of N adjustable real parameters such as capacitors, inductors, or resistors. These parameters are positive and real and will be labelled β_n. Then

$$EE^* = (D - HX)(D^* - H^*X^*) \tag{4}$$

and the change in EE^* due to the changes in $\Delta\beta_n$ is

$$\Delta EE^* = \sum_n \frac{\partial}{\partial \beta_n} (EE^*)\, \Delta\beta_n \tag{5}$$

Using Eq. (4), this becomes

$$\Delta(EE^*) = -2 \sum_n \Delta\beta_n \mathrm{Re}\ E^*X \frac{\partial H}{\partial \beta_n} \tag{6}$$

We wish to minimize the mean square error over the frequency range from ω_1 to ω_2. This will occur if we ensure that the change in the mean square error is negative, i.e., choose

$$\Delta\beta_n = \alpha_n \mathrm{Re} \int_{\omega_1}^{\omega_2} E^* X \frac{\partial H}{\partial \beta_n} d\omega \tag{7}$$

where α_n are positive constants which determine the adaptation rate. The total change in the mean square error is then

$$\int_{\omega_1}^{\omega_2} \Delta(EE^*) d\omega = -2 \sum_n \alpha_n \left[\mathrm{Re} \int_{\omega_1}^{\omega_2} E^* X \frac{\partial H}{\partial \beta_n} d\omega \right]^2 < 0 \tag{8}$$

Using the choice given in Eq. (7) for $\Delta\beta_n$, this algorithm has been implemented with good results. However, the problem with this algorithm is that α_n depends on the type of component, and it is orders of magnitude different for capacitors, inductors, and resistors. This problem can be avoided by noting that the maximum α_n for convergence is

$$\alpha_n^{\max} \leq \frac{\int EE^* d\omega}{\mathrm{Re} \left[\int E^* X \frac{\partial H}{\partial \beta_n} d\omega \right]^2} \tag{9}$$

So if we choose $\alpha_n = A\alpha_n^{\max}$ where A is independent of n and of the order of $.1$ to $.01$, then

$$\Delta\beta_n = A \frac{\int EE^* d\omega}{\mathrm{Re} \int E^* X \frac{\partial H}{\partial \beta_n} d\omega}$$

This algorithm will find the optimum component values where optimum means the least mean square error. We have chosen to use transferred power (equivalently insertion loss) for Y and have found that if the desired response D is set at 0 dB loss, then a flat frequency response is obtained. This is shown in Fig. 3 for a 3 finger pair Sezawa wave IDT. If the desired loss is set lower, for example at -2 dB loss, then ripples

in the passband are obtained (Fig. 3). Thus we should be able to obtain 43 MHz bandwidth with only 3 dB round trip electronic mismatch loss.

The original experimental and theoretical results obtained with 4 finger pair Sezawa wave IDTs are shown in Fig. 4. Also shown in that figure are the improved results obtained with the use of the optimization program.

Unbalanced IDT Excitation on Layered Media

For Rayleigh wave devices using ZnO/Si (Fig. 5a), the film thickness is ~.006 . The maximum bandwidth (minimum electronic Q) is obtained when the transducers are driven in a balanced mode. These transducers were often used in an unbalanced mode where one side of the IDT is driven and the other side grounded when initial measurements were being made and $\Delta v/v$ determined. The measurement in this case is simpler, since a balanced to unbalanced transformer is not needed. The Kino-Wagers theory could still be used to find the relation between R_a and $\Delta v/v$ since

$$R_{a_{unbal}} = (R_{a_{bal}})/4 \tag{10}$$

$$C_{T_{unbal}} = 2C_{T_{bal}} \tag{11}$$

in the limit of $\lambda/h \to 0$.

The film thickness for Sezawa waves is typically $.25\lambda$ and Eqs. (10) and (11) no longer hold since the capacitance between adjacent fingers can no longer be neglected (see Fig. 5). A strong reason for

using Sezawa wave IDTs in an unbalanced mode is that the unbalanced resistance is of the order of 150Ω instead of 600Ω and C_T is ~.7pF instead of ~.35pf . Thus matching to these transducers is much easier in the unbalanced case.

A theory has been developed and is briefly described below which predicts R_a and C_T for arbitrary voltages V_1 and V_2 being applied to the two sides of the transducer. Special cases of this theory are unbalanced excitation where one is either grounded or floating, and balanced excitation. Comparison of theoretical and experimental results are also included.

We shall first determine the capacity of the structure shown in Fig. 5 and then the radiation resistance. It is assumed that the charge is different on the two fingers of a finger pair, but that every finger pair is equivalent. A linear approximation will be used:

$$V_1 = S_{11}Q_1 + S_{12}Q_2 \tag{12a}$$

$$V_2 = S_{21}Q_1 + S_{22}Q_2 \tag{12b}$$

where S_{11} is independent of Q_1 . The derivation is simpler if we assume the finger widths and spacings are the same for all the fingers. In this case, $S_{11} = S_{22}$ and $S_{12} = S_{21}$. The more general case is easily solved using the same techniques. The two unknowns S_{11} and S_{12} can be found by considering two special cases where the relationship between V_i and Q_i can be explicitly calculated.

Balanced excitation is the first special case considered:

$$Q_2 = -Q_1$$

$$V_1 = (S_{11} - S_{12})\, Q_1$$

This case was worked out by Kino and Wagers[6] with the result

$$\frac{1}{C_s} \approx \frac{(2V_1)}{Q_1} = 2(S_{11} - S_{12})$$

$$\frac{1}{C_s} = \frac{4}{\pi w} \sum_0^\infty \left(\frac{\sin\ (2m+1)\ \frac{\pi d}{\ell}}{(2m+1)\ \frac{\pi d}{\ell}} \right) \frac{1}{(2m+1)\varepsilon_0 + \varepsilon_p^1 \coth \gamma h} \qquad (13)$$

where C_s is the capacity per finger pair, $(2V_1)$ is the total voltage across the capacitor, d is the width of the finger, and ℓ is the repeat distance of the transducer.

For the second special case, consider the case when one side of the transducer is disconnected, i.e. $Q_2 = 0$. Then

$$V_1 = S_{11} Q_1$$

As shown in ref. 6, the finger capacity can be expressed in the form

$$C_s = \frac{Q^2}{w \int_0^\ell \sigma \phi dX}$$

To find the relation between σ and ϕ, it is easier to work in the Fourier transform domain and solve Laplace's equation in the three regions (substrate, film, and air), and match boundary conditions. The derivation is similar to that of ref. 6 except that there is a term in σ_k and ϕ_k with no spatial frequency variation, and the solution of Laplace's equation is different in this case. The result of the calculation is

$$S_{11} = \frac{h}{\varepsilon_{zz}^1 w \ell} + \frac{1}{\pi w} + \sum_{n=1}^\infty \frac{1}{n} \left(\frac{\sin \frac{n\pi d}{\ell}}{\frac{n\pi d}{\ell}} \right)^2 \frac{1}{\varepsilon_0 + \varepsilon_p^1 \coth \gamma h}$$

Using Eq. (13), S_{12} can be found

$$S_{12} = \frac{h}{\epsilon^I_{zz} w \ell} + \frac{1}{\pi w} \sum_{m=1}^{\infty} \frac{1}{2m} \left(\frac{\sin \frac{2m\pi d}{\ell}}{\frac{2m\pi d}{\ell}} \right)^2 \frac{}{\epsilon_0 + \epsilon^I_p \coth \gamma^I_{2m} h}$$

$$- \frac{1}{\pi w} \sum_{m=0}^{\infty} \frac{1}{(2m+1)} \left(\frac{\sin \frac{(2m+1)\pi d}{\ell}}{\frac{(2m+1)\pi d}{\ell}} \right)^2 \frac{1}{\epsilon_0 + \epsilon^I_p \coth \gamma_{(2m+1)} h}$$

Note that $S_{12} < 0$ as expected, and that these series converge very rapidly (as $1/n^3$).

We can now calculate the capacitance of the IDT in an unbalanced mode with one side floating

$$C_f = \frac{N}{S_{11}}$$

or with one side grounded

$$C_g = \frac{N}{S_{11}} \left(1 - \frac{S^2_{12}}{S^2_{11}} \right)$$

The capacitance in these cases is plotted in Fig. 6 as a function of film thickness for 3 different repeat distances. The finger widths

and spacings are $\ell/4$ in this calculation. For a film thickness less than $.25\lambda$, it doesn't matter whether the opposite finger is floating or grounded.

To derive the expression for radiation impedances, we use the expression for the amplitude of the forward propagating wave

$$a(L) = A(Q_1 - Q_2)$$

where

$$A = \alpha\left(\frac{\sin\frac{Nkd}{2}\ \sin\frac{k\ell}{2}}{\sin\frac{k\ell}{2}\ \frac{kd}{2}}\right)$$

The radiation impedance is[7]

$$Z_A = \frac{Za(L)a(L)^*}{I_1 I_1^*} \tag{14}$$

$$Z_A = \frac{R_{a0}F(\omega)}{4|Q_1|^2}|Q_1 - Q_2|^2$$

where

$$R_{a0} = \frac{4\frac{sv}{v}}{w\omega_0(\epsilon_0 + \epsilon_p \coth \gamma h)}\left(\frac{\sin\frac{\pi d}{\ell}}{\frac{\pi d}{\ell}}\right)^2$$

and

$$F(w) = \left(\frac{\sin x}{x}\right)^2 + j\frac{\sin 2x - 2x}{2x^2}$$

In the balanced mode, $Q_1 = -Q_2$ and $Z_a = R_{a0}F(\omega)$, just as Kino and Wagers[6] obtained.

When one side is grounded, we use the weak coupling approximation, i.e., Q is determined from electrostatic considerations

$$V_2 = 0 = S_{12}Q_1 + S_{11}Q_2$$

$$Q_2 = \frac{-S_{12}}{S_{11}} Q_1$$

Thus, using Eq. (14)

$$Z_a = \frac{R_{a0}F(\omega)}{4}\left(1 + \frac{S_{12}}{S_{11}}\right)^2$$

In the limit $h \to 0$, for $d/\ell \ll 1$, $S_{12} \to 0$ and

$$Z_a \approx \frac{R_{a0}F(\omega)}{4} \qquad (h \approx 0)$$

as expected. In the limit $h \to \infty$, then $S_{12}/S_{11} \to 1$ and

$$Z_a \approx R_{a0}F(\omega) \qquad (h/\lambda \gg 1)$$

which is the result obtained by Kino and Wagers.[6]

For the case of one side floating, $Q_2 = 0$ and

$$Z_A = \frac{R_{a0}F(\omega)}{4}$$

The ratio of the radiation resistance in the unbalanced case to the balanced case is shown in Fig. 7.

The experimental results for radiation resistance and capacitance are also shown in Fig. 6. The agreement with the theoretical values is good. Note that the radiation resistance is increased by 25% when the opposite fingers are grounded for the case of 16 μm periodicity transducers. The conclusions of this theory for Rayleigh wave and Sezawa wave devices are given in Table I. Note that the results of this theory are important for the Sezawa wave case, but unimportant for our Rayleigh wave devices since the film thickness is significantly smaller.

B. Schottky Diode Devices

We have demonstrated the feasability of a monolithic Schottky diode storage correlator. The operation of this device is similar to that of the pn diode storage correlator, with the advantage of having the ideal diode transient response characteristic of the Schottky diode. We have performed experiments that indicate that it is indeed possible to store signals in the Schottky diode correlator within a single short pulse of a duration of approximately one half rf cycle. Figures 8 and 9 indicate the autocorrelation of a square pulse approximately 4.5 μsec long, and 2 volts in amplitude. In Fig. 8, a 6 nsec 7 volt pulse was applied to the top-plate to store the pulse, and the pulse was read out approximately 50 μs later with a 5 μsec , .75 volt rf modulated pulse on the top plate. In Fig. 9 the output correlation of the stored

signal with the readout signal is observed. We have found that a new containment box fabricated specifically for these devices has been extremely effective in reducing the rf feedthrough signals that so often plague these devices.

We have also carried out work on improving the efficiency of these devices. Apart from the work done on optimizing the deposition conditions for ZnO films, mentioned elsewhere in this report, we have investigated some of the other loss mechanisms in the storage correlator. We have found that the gold film, used for metallization of the top plates of these devices, tends to give excessive loss, this is thought to be due to scattering from grain boundaries in the polycrystalline gold films. These losses vary over a wide range depending on the precise deposition conditions of the gold films, but are typically of the order of 3 dB per centimeter with a 1000Å gold film. These losses are far above the theoretical values that would be attributed to the viscosity of the gold film. We have found that aluminum top plates offer a great improvement in this respect, reducing the propagation loss to essentially negligible values. Improvements in insertion loss from 30 to 24 dB have been observed by merely switching to aluminum top plates.

When the correlator is operated in the short pulse storage mode, the limitation on the storage time is given not by the characteristic of the diode itself, but by the series resistance that the diode sees between itself and the voltage source.

It is important that the RC time constant of this resistance in series with the capacitance of the top plate be kept to a minimum. For this reason, we have begun investigating the possibility of fabricating devices in n-type epitaxial layers grown in highly doped n+ substrates. Preliminary tests indicate that the required epi thicknesses and dopant concentration levels are within the capabilities of already existing deposition facilities at Stanford, and we are now developing depth profiling routines to confirm that the desired doping profiles have been achieved.

We are constructing a further series of Schottky diode devices with lower leakage current at the diodes with a more careful use of processing. Leakage current in these Schottky diode devices has been a major problem as compared to the equivalent air-gap devices.

We are also investigating an alternative system for Schottky diode devices, making the use of polysilicon deposited on lithium niobate ($LiNbO_3$), which is then laser annealed. Two sets of experiments will be carried out in cooperation with Prof. Gibbons. The first is the deposition of SiO_2 on $LiNbO_3$ to protect the lithium niobate, and then the deposition of polysilicon on the SiO_2. These experiments will be run to determine whether we can indeed deposit polysilicon on the lithium niobate without cracking it. If we can do this, Gibbons is confident that we can develop annealed silicon with a very low surface density. Thus, if we are successful in producing silicon on lithium niobate, we should have excellent device quality, provided the acoustic losses are not too great. Thus, if they succeed in producing silicon on lithium niobate, we will go forward immediately to put transducers on

the same substrate and test acoustic loss and the performance of the device as a convolver.

The second set of experiments are concerned with whether we can put Schottky diodes on the underside of the silicon so as to make a storage correlator. The basic idea will be to deposit platinum layers on the silicon dioxide, then deposit the polysilicon, thus forming Schottky diodes in the annealed silicon. We will try this first with a silicon substrate as the idea has merit for its own sake.

Our ultimate intention is to make a high-quality Schottky diode storage correlator which has a fast turn-on time. It is our aim, of course, to make a monolithic correlator. So far, ZnO has appeared to be the best way to carry this out, but since there is a long time period between runs, there is time without use of much additional manpower to carry out these investigations on lithium niobate. Our feeling is that it would be unwise to neglect the laser annealing approach, for it might provide major breakthroughs in the surface wave field.

C. ZnO Technology Development

Using our new planar discharge sputtering ZnO system, we are continuing our characterization of ZnO films sputtered at high substrate temperatures up to 450°C . Our best results, as measured by the tuned round trip insertion loss of a sapphire delay line, were obtained at a substrate temperature of 450°C . The following table summarizes these results.

T_{sub}	F_0	I.L.
450°C	300 MHz	3 dB
	500 MHz	5 dB
	1 GHz	7 dB
	2 GHz	11 dB

We found that the same insertion loss is obtained with different material backing layers such as Au, Pt, and Al; as long as these metals are well oriented. We have had problems depositing well-oriented ZnO on Au for our surface wave work. This problem was due to the poor orientation of the gold film. This poor orientation of the gold was due to an unintentional change in one of the deposition parameters due to a change in the substrate holder. This difficulty has been corrected and we should be able to make surface wave devices without any problems.

We have carried out a calculation on the sputtering profile from a planar magnetron discharge sputtering system, to determine the target substrate spacing for maximum uniformity of sputtered fibers. We assume that the sputtering from the erosion ring follows a cosine law distribution (a valid assumption for high-energy sputtering). Fig. 10 is a plot of the normalized thickness versus distance from the target on axis ($r = 0$). Fig. 11 is a plot of the thickness profiles of the sputtered film versus radial distance away from the center of the target, for various distances z_0 away from the target. The thickness is normalized to its value at $r = 0$. For optimum uniformity of the sputtered film, the target substrate spacing should be equal to 1.3 times the radius of the erosion ring. It is obvious from Fig. 10 that by decreasing our present substrate target spacing from 7.5 cm to 5 cm, we could double

our sputtering rate and improve the uniformity to better than 1% over a region with a diameter of 6 cm . We are presently setting up an

In order to obtain the optimum sputtering conditions, we have started a detailed study to evaluate the quality of ZnO thin films sputtered under different conditions, using x-ray diffractometry, R.E.D, S.E.M on the surface and on a fracture edge, and resistivity measurements.

REFERENCES

1. Hsing Tuan, Ph.D. thesis, Stanford University, 1980.
2. B. T. Khuri-Yakub and R. Joly, El. Lett.
3. B. T. Khuri-Yakub, Ph.D. thesis, Stanford Univ., 1975.
4. H. W. Bode, Network Analysis and Feedback Amplifier Design, Van Nostrand, New York, 1945.
5. R. M. Fano, J. Franklin Inst. 249, 57 (1950).
6. G. S. Kino and R. S. Wagers, J. Appl. Phys., 44, 1980 (1973).
7. G. S. Kino, Theory of Acoustic Devices, Prentice Hall, to be published.

TABLE I

Summary of Transducer Parameters for Present Devices

Type	Mode	$R/(R_{a0}F(\omega))$	C/C_{bal}
Sezawa Wave Devices	balanced	1	1
(h = 8 μm , d = 32 μm ,	floating	.25	1.75
d = 8 μm)	grounded	.31	1.80
Rayleigh Wave Devices	balanced	1	1
(h = 8 μm , d = 32 μm ,	floating	.25	2
d = 8 μm)	grounded	.25	2

FIGURE CAPTIONS

1. Minimum loss versus bandwidth for an ideal tuning network.

2. Generalized network and load (IDT) used in least mean square optimization algorithm.

3. Insertion loss versus frequency for a 3-finger pair Sezawa wave IDT for a network which gives minimum ripple (solid) and a network which gives maximum 3 dB bandwidth.

4. Insertion loss versus frequency for a 4-finger pair Sezawa wave IDT showing the original theoretical and experimental results, and results of using the optimization program.

5. Schematic drawing of a) device with $h/\lambda = .006$ (Rayleigh wave device); and b) device with $h/\lambda = .25$ (Sezawa wave device).

6. Capacitance versus film thickness for unbalanced transducers. a) $w = 1$ mm ; b) $w = 6$ mm .

7. Ratio of the radiation resistance in the unbalanced and balanced cases versus film thickness.

8. Pulse used to store acoustic signal in storage correlator:
   10 nsec per horizontal division
   2 volts per vertical division.

9. Storage correlation output with 4 dB of gain in system:
   .02 volts per vertical division
   2 μsec per horizontal division.

10. Normalized thickness versus distance from target on axis ($r = 0$) .

11. Thickness profiles of sputtered film versus radial distance away from center of target.

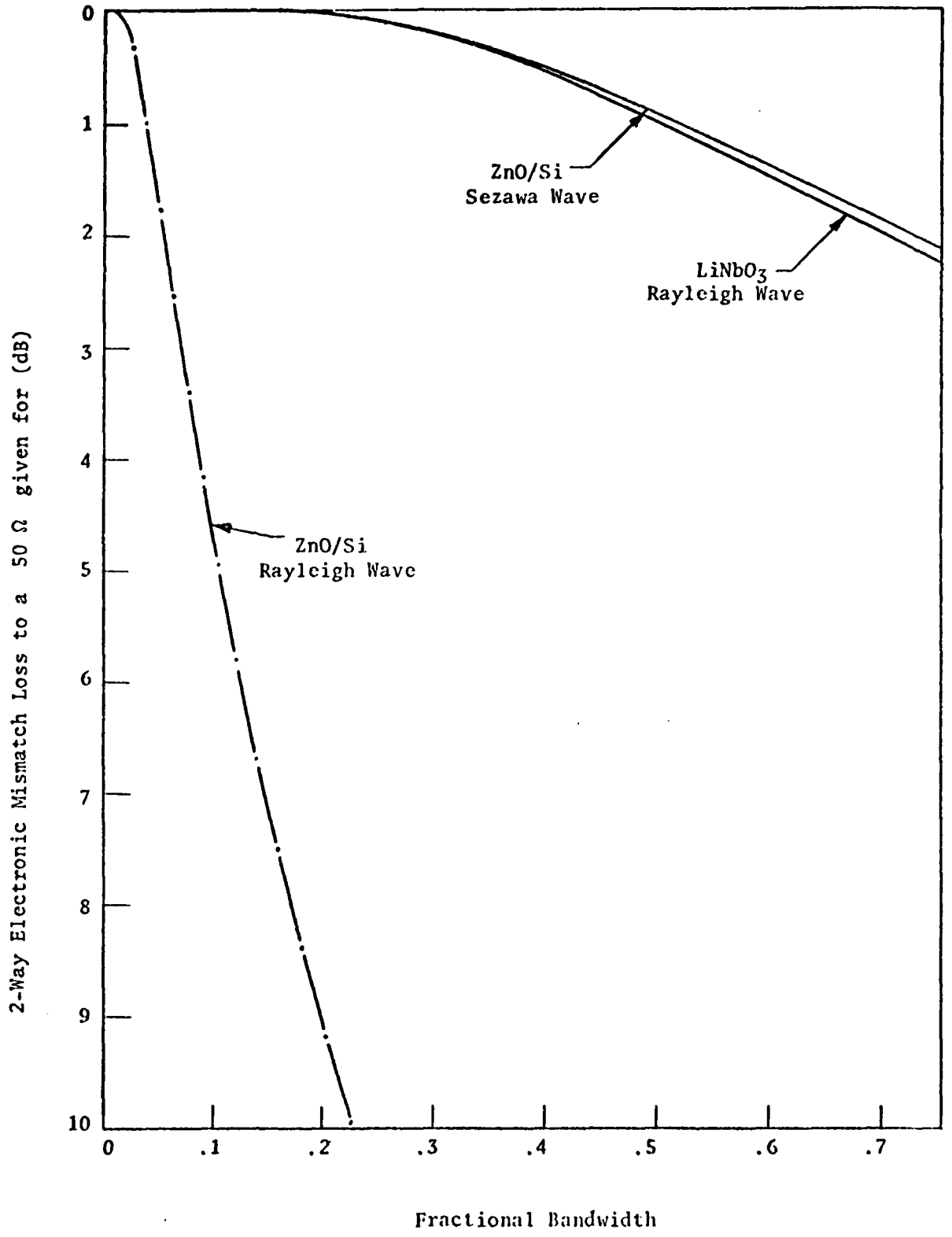
0
1
2
3
4
5
6
7
8
9
10
2-Way Electronic Mismatch Loss to a 50 Ω given for (dB)
ZnO/Si
Sezawa Wave
LiNbO3
Rayleigh Wave
ZnO/Si
Rayleigh Wave
0
.1
.2
.3
.4
.5
.6
.7
Fractional Bandwidth

Fig. 1

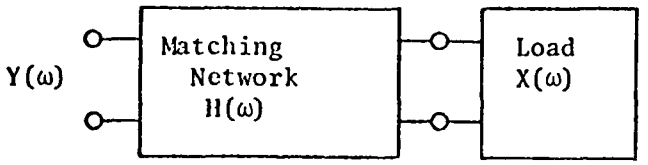

Fig. 2

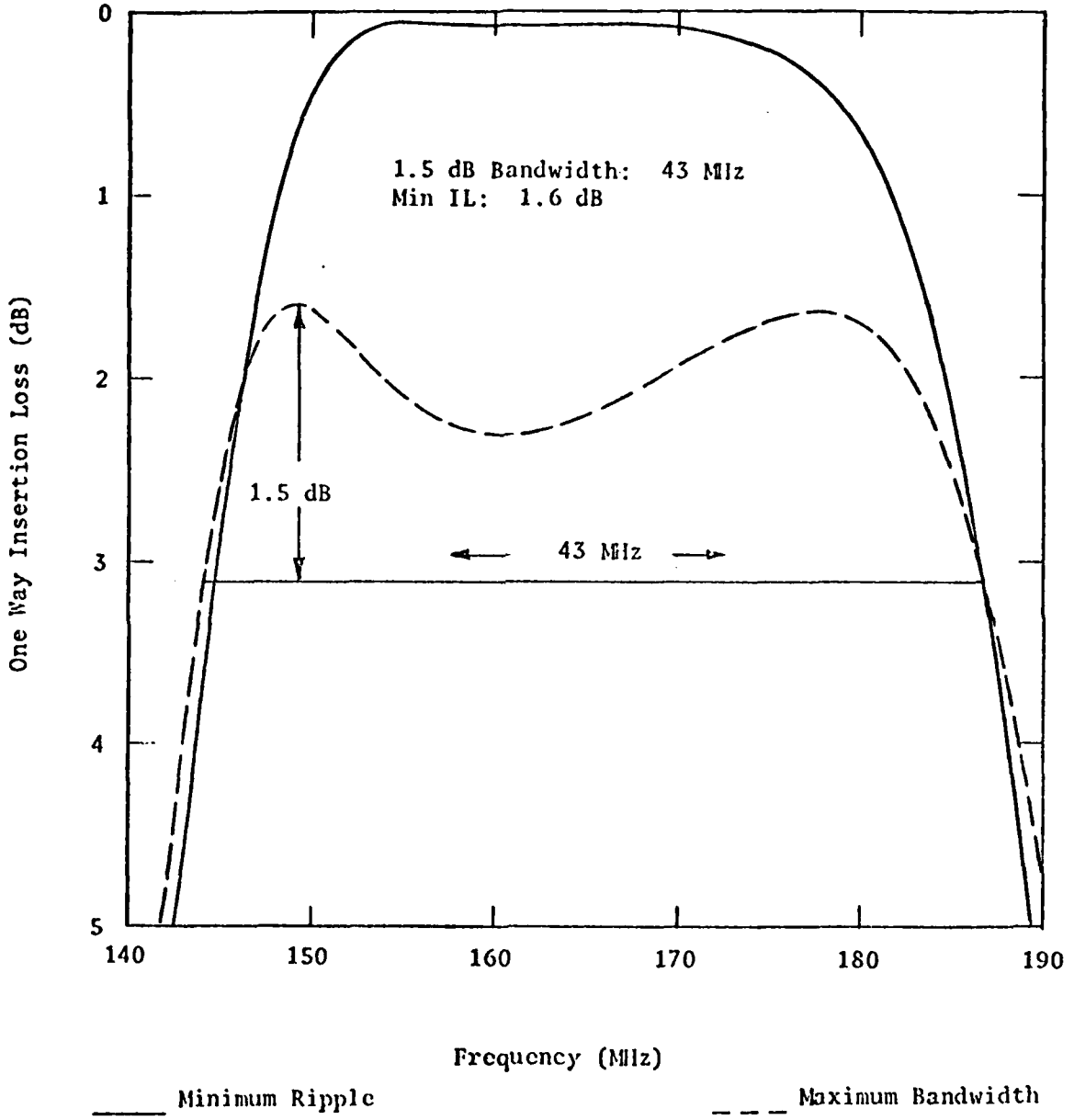
0
1
2
3
4
5
One Way Insertion Loss (dB)
1.5 dB Bandwidth: 43 MIz
Min IL: 1.6 dB
1.5 dB
43 MIz
140
150
160
170
180
190
Frequency (MIz)
Minimum Ripple
Maximum Bandwidth

Fig. 3

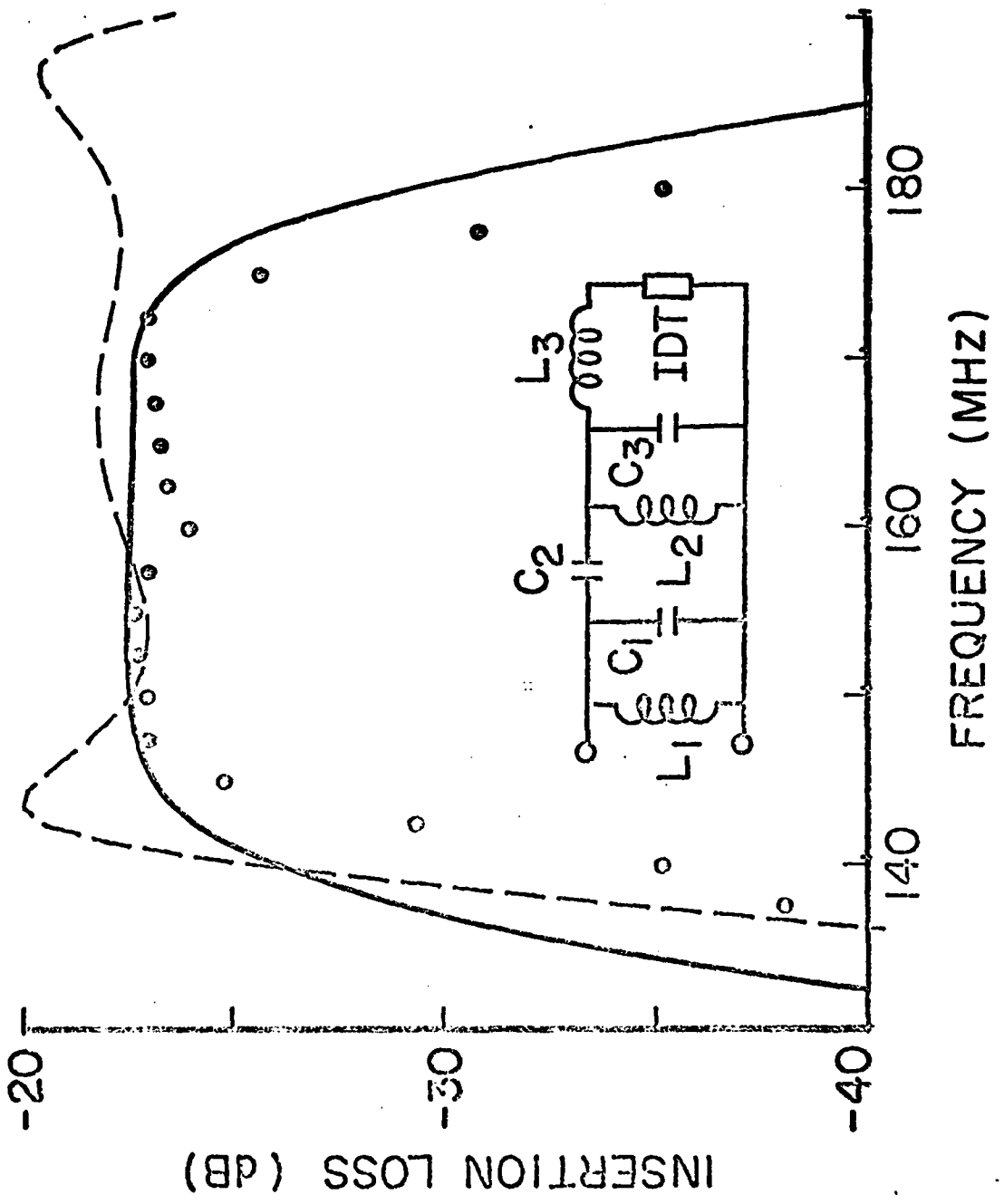
INSERTION LOSS (dB)
-20
-30
-40
FREQUENCY (MHz)
140
160
180
L3
IDT
C3
L2
C2
C1
L1

Fig. 4

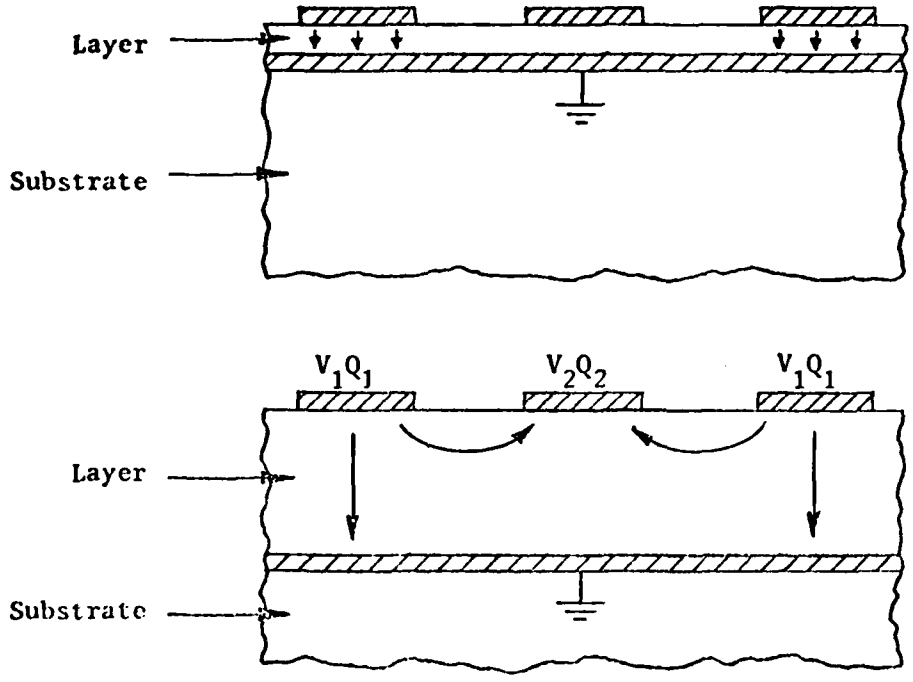

Fig. 5

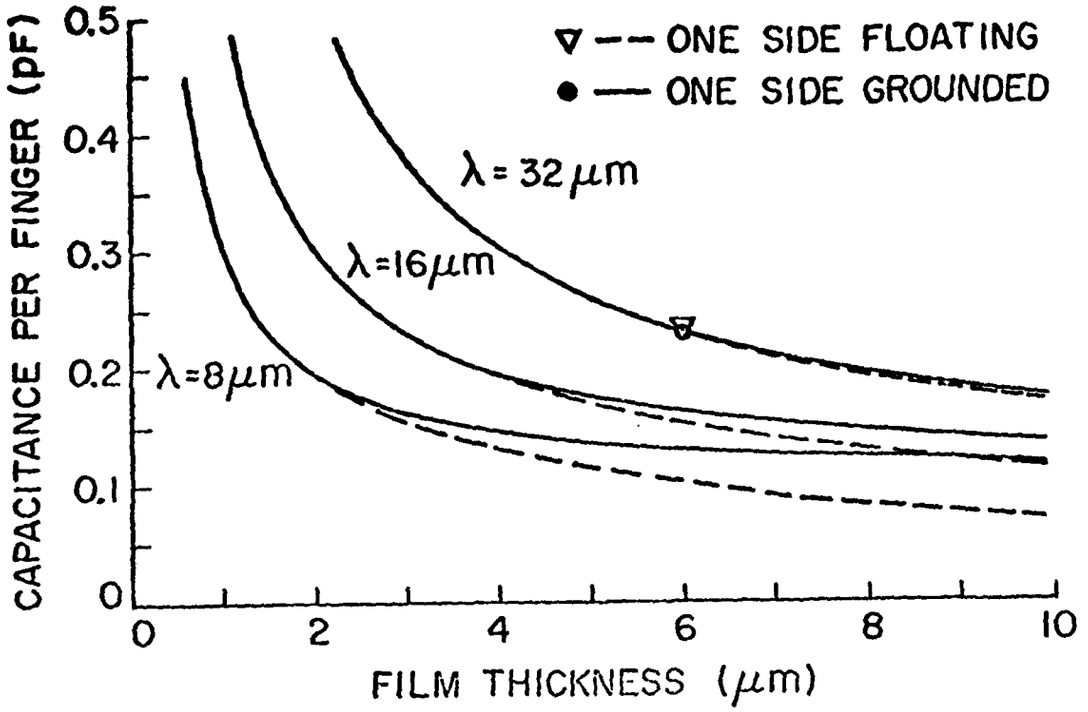
▽ — — ONE SIDE FLOATING
● —— ONE SIDE GROUNDED
λ = 32 μm
λ=16μm
λ=8μm
CAPACITANCE PER FINGER (pF)
0.5
0.4
0.3
0.2
0.1
0
0
2
4
6
8
10
FILM THICKNESS (μm)

Fig. 6a

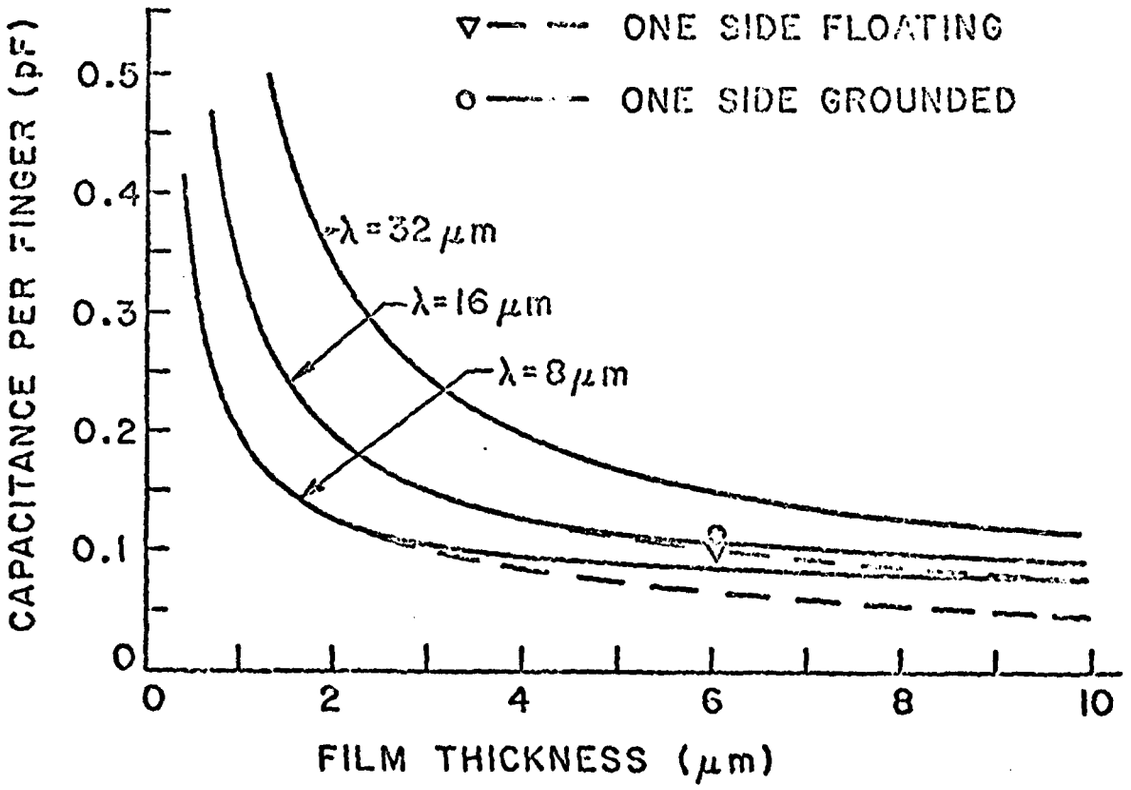
▽— — ONE SIDE FLOATING
o— - — ONE SIDE GROUNDED
λ=32 μm
λ=16 μm
λ=8 μm
CAPACITANCE PER FINGER (pF)
0.5
0.4
0.3
0.2
0.1
0
0
2
4
6
8
10
FILM THICKNESS (μm)

Fig. 6b

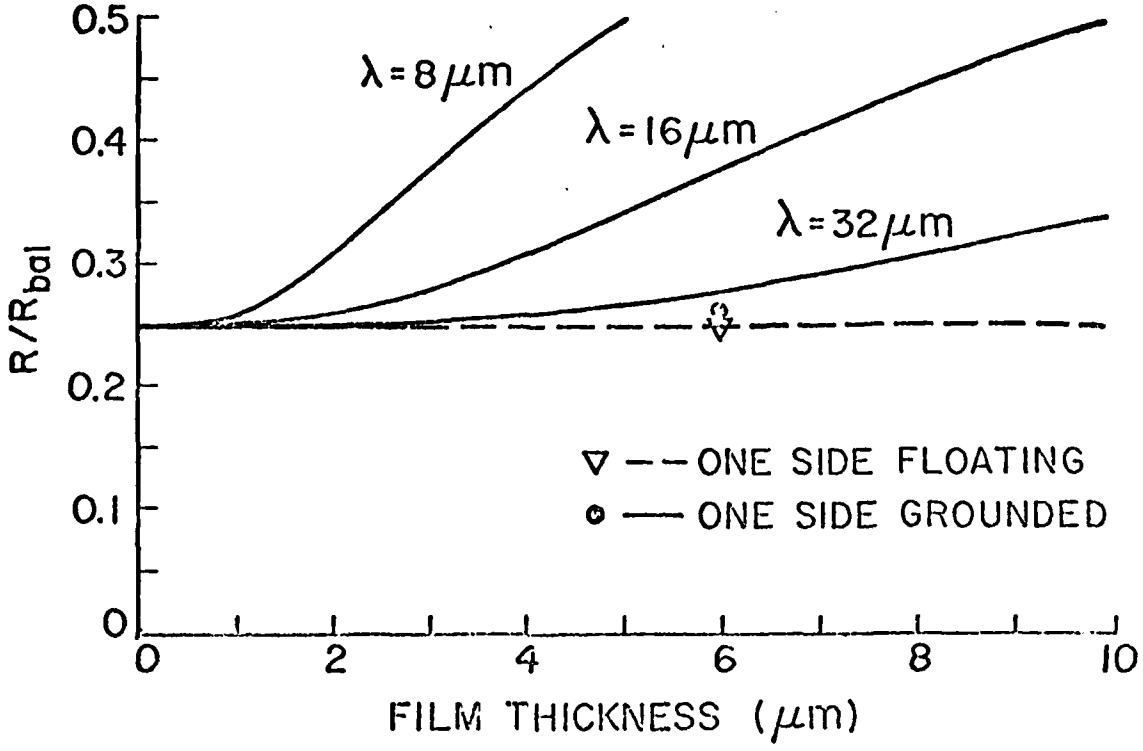
0.5
0.4
0.3
0.2
0.1
0
R/R_bal
λ=8μm
λ=16μm
λ=32μm
▽ -- ONE SIDE FLOATING
⊙ — ONE SIDE GROUNDED
0
2
4
6
8
10
FILM THICKNESS (μm)

Fig. 7

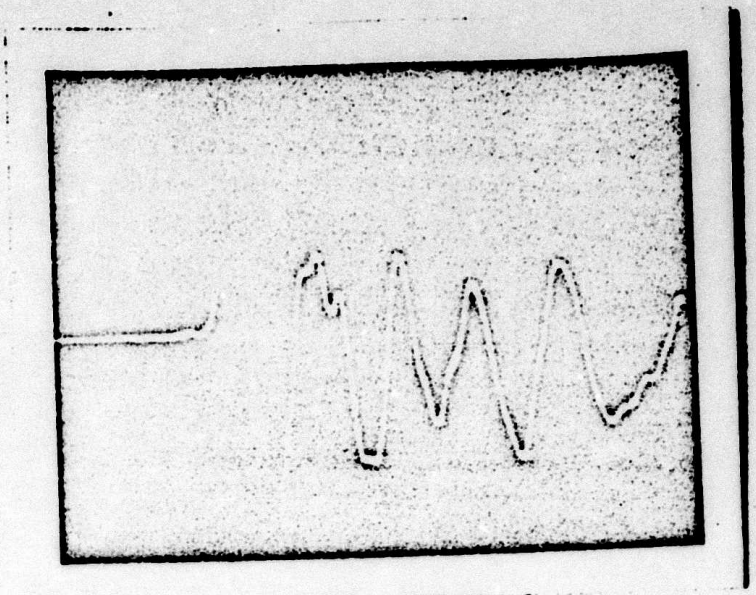

Fig. 8

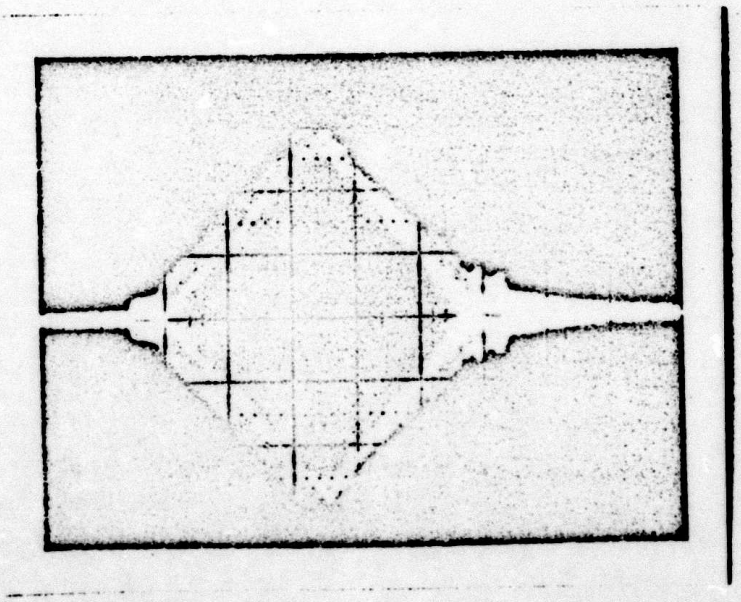

Fig. 9

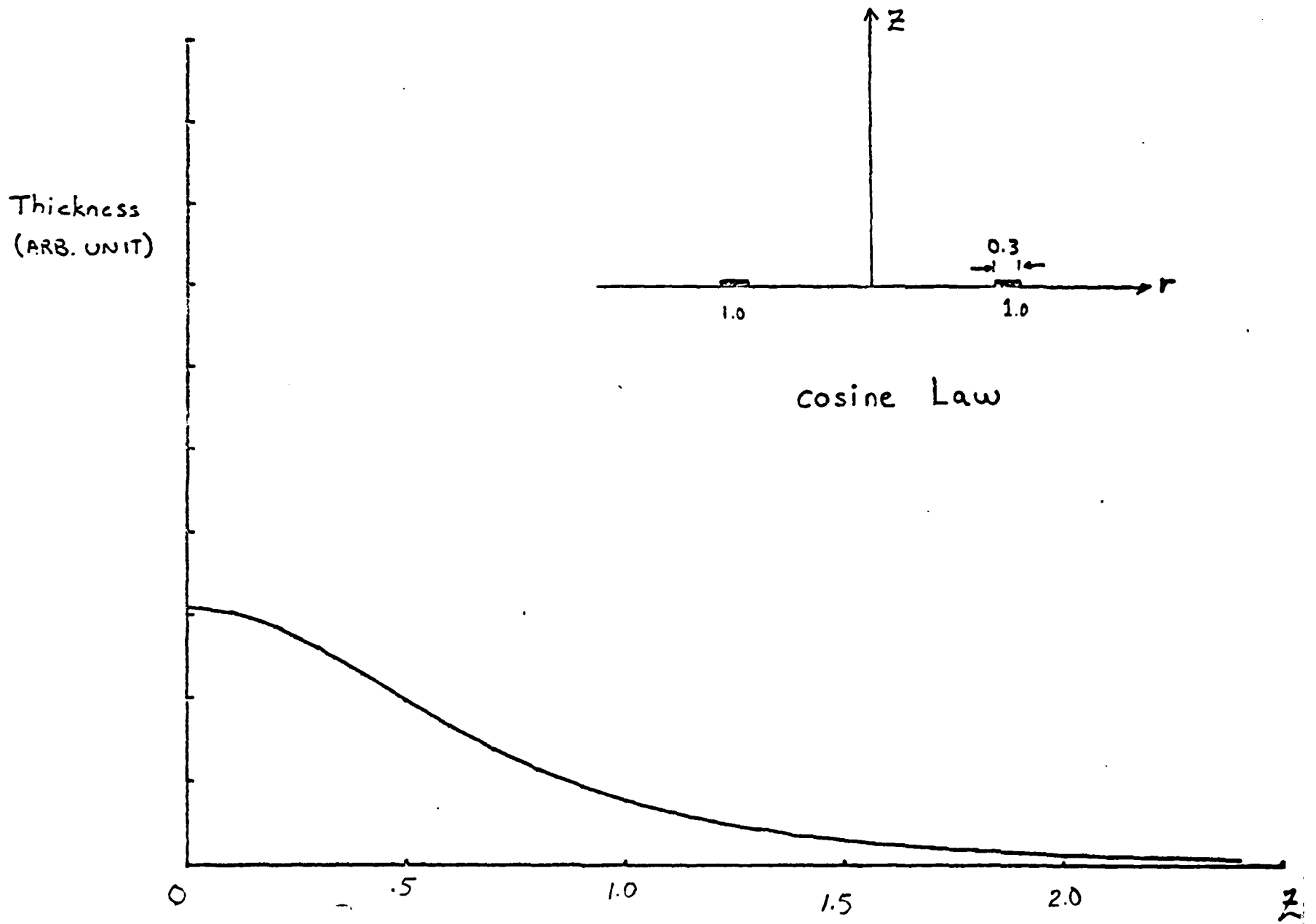

Fig. 10

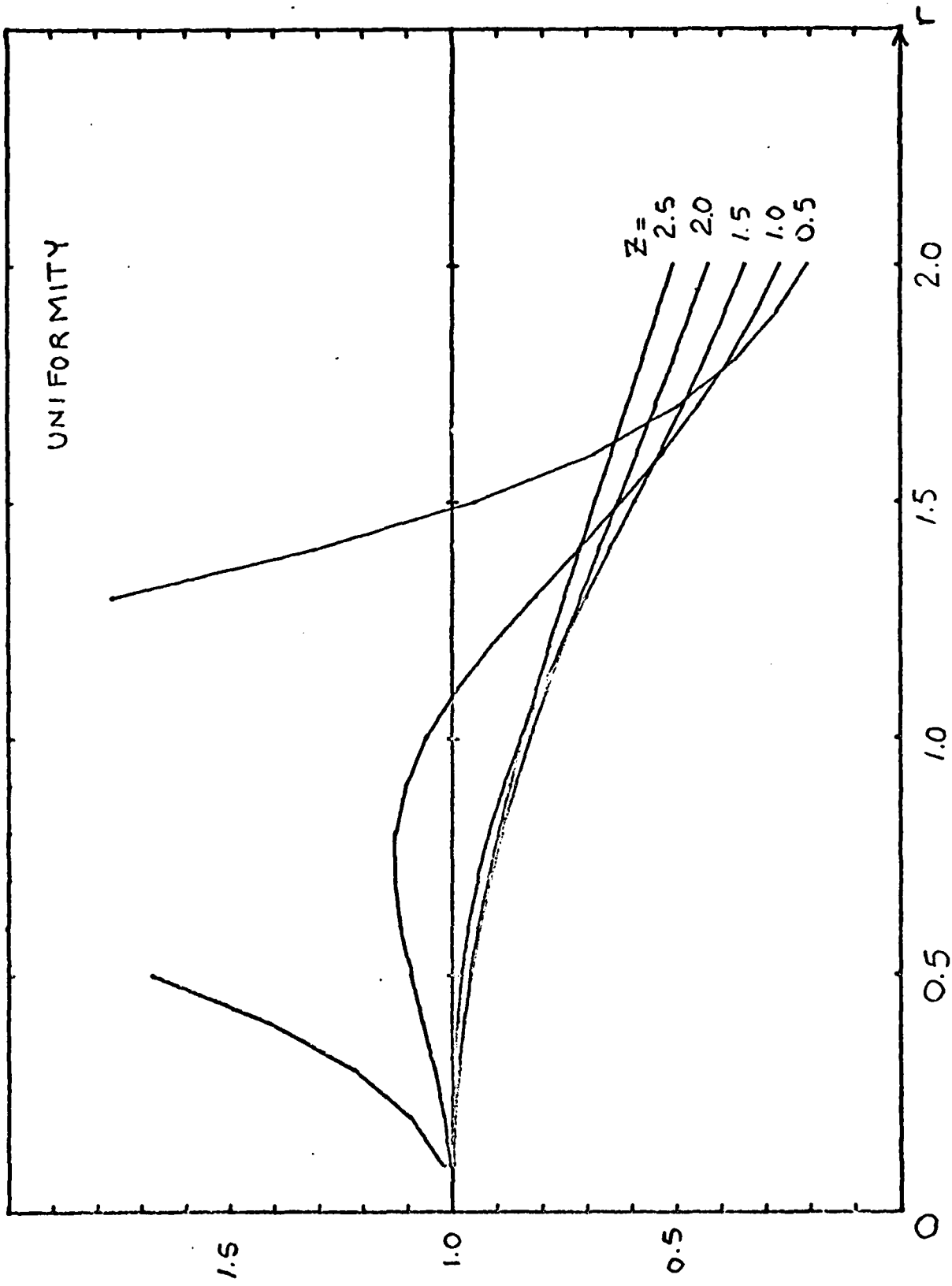

Fig. 11

APPENDIX I

BROADBAND, EFFICIENT, THIN FILM SEZAWA WAVE IDTS

J. E. Bowers, B. T. Khuri-Yakub, and G. S. Kino

Abstract

The phase velocities and coupling coefficients for Sezawa waves in (001) ZnO on (001) cut, (100) prop. Si and on (111) cut, ($11\bar{2}$) prop. Si are presented. Experimental results from Sezawa wave delay lines are presented which represent for the first time bandwidths in excess of 30 MHz in a thin film monolithic device.

Acoustic surface wave (ASW) signal processing devices such as convolvers and storage correlators can be monolithic, thin film devices (typically ZnO on Si)[1] or hybrid arrangements where a piezoelectric substrate (typically $LiNbO_3$) is pressed against a semiconductor (typically Si).[2,3] The monolithic approach has the advantages of ruggedness, smaller size, and fewer spurious signals, and the devices are fabricated using standard planar processing and are potentially much cheaper to make. The very important limitation of monolithic ASW devices has been the inherent narrow fractional bandwidth (10-15%) which is a result of the low coupling coefficient ($\Delta v/v \leq .004$) attainable with thin film Rayleigh wave devices. Larger first order Rayleigh wave coupling coefficients ($\Delta v/v \leq .015$) are attainable with thicker films ($h \sim .5\lambda$ rather than $h \sim .007\lambda$).

Armstrong and Crampin[5] have presented theoretical calculations for the coupling coefficient of second order Rayleigh waves, commonly called Sezawa waves[6] for (001) ZnO on (001) Si. They found a peak coupling coefficient of .024 at a velocity of 4921 m/s . Elliot et al.[7,8] have made Sezawa wave signal processing devices with 13% bandwidth.

In this paper, we present theoretical and experimental values for the phase velocity and coupling coefficient for Sezawa waves in (001) ZnO on (001) and (111) Si. Information is also presented on the third order Rayleigh mode on (001) Si. Finally, results are presented on Sezawa wave delay lines with fractional bandwidths of 19 and 25% at a center frequency of 165 MHz.

The dependence of phase velocity on the thickness h of the different surface acoustic waves that are possible in a film of (001) ZnO on a (001) cut, 100 prop. Si substrate are shown in Fig. 1. The Sezawa mode is

cut off at the silicon shear wave velocity, which is 5800 m/s for this orientation and propagation direction. This mode is progressively more lossy as k is decreased below the cut-off value ($k_c = .73$). The cut-off value varies by as much as 15%, depending on the electrical conditions at the surface and the film-substrate interface.

The coupling coefficients of the Sezawa mode are shown in Fig. 2 for the four possible transducer configurations. Note that we predict coupling coefficients as large as .028, which is six times larger than the first Rayleigh wave peak for this orientation.[4]

The coupling coefficient $\Delta v/v$ must be calculated at a constant value of ω, not k as in Armstrong and Crampin[5], since the theories[4,9] for transducer impedance all use $\Delta v/v$ at constant ω. Our calculations for $\Delta v/v$ at constant k agree with the results of Armstrong and Crampin[5] and yield a value for the peak coupling coefficient which is 17% lower than the correct value. Armstrong and Crampin report a phase velocity of 4921 m/s, which is significantly lower than our theoretical and experimental results and the experimental results of Elliot et al.[7]

The first order Rayleigh wave coupling coefficient is .0002 at the optimum film thickness for Sezawa wave coupling ($hk = 1.65$) for transducers at the free surface and a metal shorting plane at the interface. Thus, the spurious Rayleigh wave generation is 50 dB smaller. The coupling coefficient for Love waves to these transducers is zero, so these waves are not excited.

The maximum coupling coefficient for third order Rayleigh waves was found to be .0072 at $hk = 5.8$. This mode is cut off at $hk = 3.2$ and is not desirable for these applications because of the low coupling coefficient.

The Sezawa wave phase velocity and coupling coefficient for (111) cut ($11\bar{2}$) prop. Si are shown in Figs. 3 and 4, respectively. The silicon shear wave velocity is lower (5000 m/s) for this orientation and propagation, and, consequently, the cut-off occurs at a higher value of hk: 2.15 .

We have built Sezawa wave delay lines on both the (001) and (111) orientations. The experimental agreement with theoretical values for phase velocity (Figs. 1 and 3) and coupling coefficient (Fig. 2) is good.

Using the coupled resonator tuning network shown in Fig. 5, a 3 dB bandwidth of 31 MHz with 22.8 dB insertion loss was achieved (Fig. 5). The device parameters are given in Table I. The theoretical plot of insertion loss was obtained using the theoretical values for phase velocity and $\Delta v/v$ and the measured values given in Table I for the device and network parameters. The equations for transducer impedance and capacitance derived by Kino and Wagers[4] for balanced excitation were modified to apply to the case of unbalanced excitation. Using a 2-stage π network,[10] bandwidths as large as 42 MHz were attained, although the insertion loss was higher (35 dB).

In conclusion, theoretical and experimental values for the phase velocities and coupling coefficients are presented here. Bandwidths in excess of 30 MHz were achieved for the first time in a monolithic ZnO on Si device.

The authors wish to thank R. Wagers and M. Drake for their help and guidance with the computer calculations. The computer calculations were made using a program developed at Stanford[11] and used the crystal constants compiled by Auld.[12] This work was supported by the Defense Advance Research Program Agency and monitored by the Office of Naval Research under Contract No. N00014-76-C-0129.

REFERENCES

1. H. C. Tuan and G. S. Kino, Appl. Phys. Lett., 31, 641, 1977.

2. K. A. Ingebritsen, R. A. Cohn, and R. W. Mountain, Appl. Phys. Lett., 26, 596, 1975.

3. C. Maerfeld and Ph. Defranould, IEEE Ultrasonics Symp. Proc., 208, 1975.

4. G. S. Kino and R. Wagers, J. Appl. Phys., 44, 1480, 1973.

5. G. A. Armstrong and S. Crampin, Electr. Lett., 9, 322, 1973.

6. K. Sezawa, Bull. Earthquake Res. Inst., 3, 1, 1927.

7. J. K. Eliott, R. L. Gunshor, R. F. Pierret, and A. R. Day, Appl. Phys. Lett., 32, 515, 1979.

8. F. C. Lo, R. L. Gunshor, and R. F. Pierret, Appl. Phys. Lett., 34, 725.

9. W. R. Smith, H. M. Gerard, J. H. Collins, T. M. Reeder, and H. J. Shaw, IEEE Trans. Microwave Theory, Tech., 17, 865, 1969.

10. T. M. Reeder, W. R. Shreve, and P. L. Adams, IEEE Trans. Sonics Ultrasonics, 19, 466, 1972.

11. R. Wagers, Ph.D. dissertation, Stanford University, 1972.

12. B. A. Auld, Acoustic Fields and Waves in Solids, vol. 1, 357 1973.

TABLE I

Delay Line Parameters

Substrate orientation: (001)	L_1 = .048 μm
Number of finger pairs: 4	L_2 = .048 μm
Wavelength: 32 μm	L_3 = .9 μm
Film thickness: 8 μm	C_1 = 36 pF
Beam width: 1 mm	C_2 = 40 pF
Pad capacitance: .2 pF	C_3 = 9.6 pF

FIGURE LEGENDS

Fig. 1 Phase velocity versus normalized filter thickness of (001) ZnO on (001) cut (100) prop. Si.

Fig. 2 Sezawa wave coupling coefficient versus normalized film thickness for (001) ZnO on (111) cut, $(11\bar{2})$ prop. Si.

Fig. 3 Phase velocity versus normalized film thickness for (001) ZnO on (111) cut $(11\bar{2})$ prop. Si.

Fig. 4 Sezawa wave coupling coefficient versus normalized film thickness for (001) ZnO on (111) cut, $(11\bar{2})$ prop. Si.

Fig. 5 Insertion loss versus frequency of a Sezawa wave delay line on (001) cut (100) prop. Si.

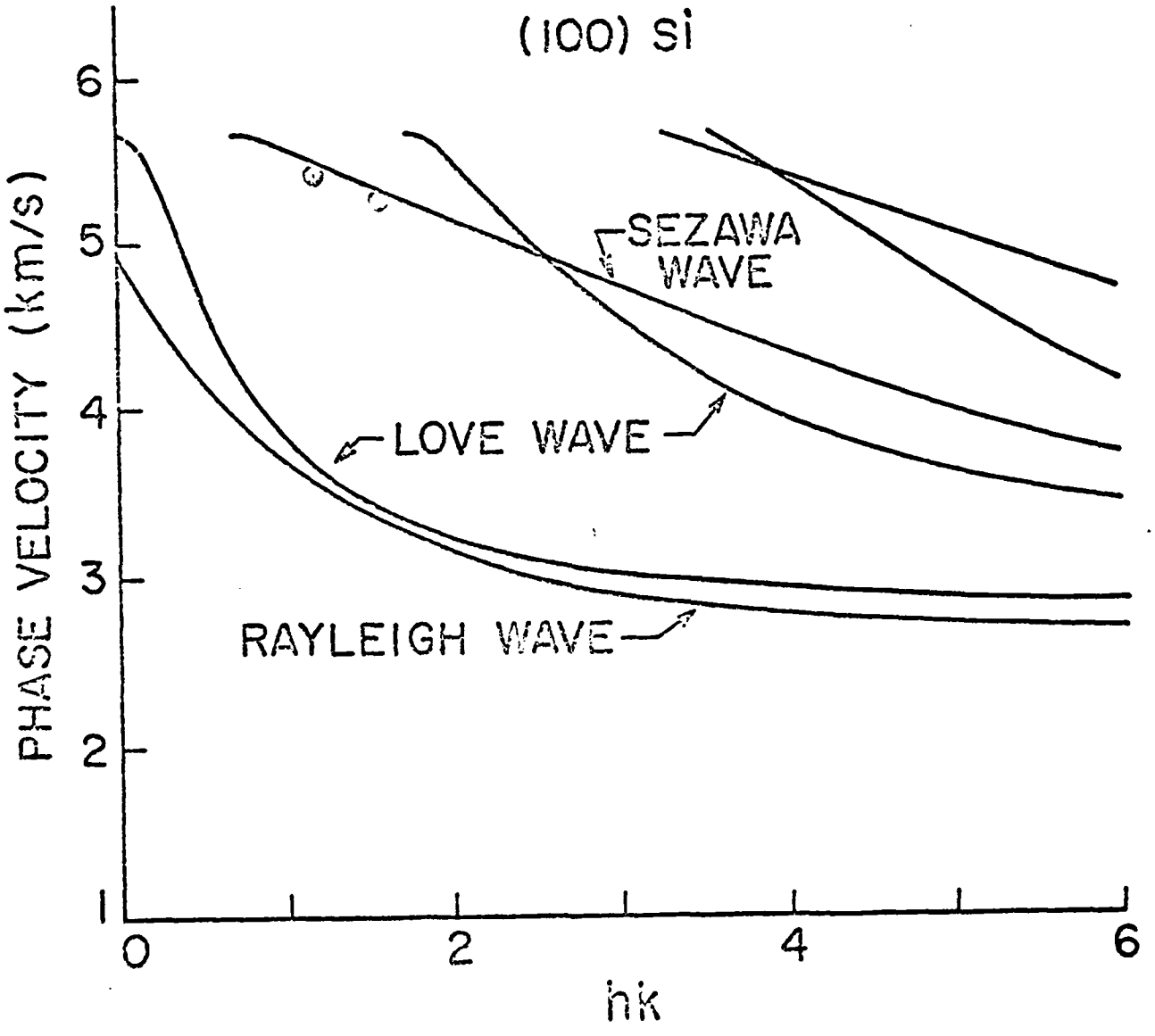
(100) Si
PHASE VELOCITY (km/s)
6
5
4
3
2
1
0
2
4
6
hk
SEZAWA WAVE
LOVE WAVE
RAYLEIGH WAVE

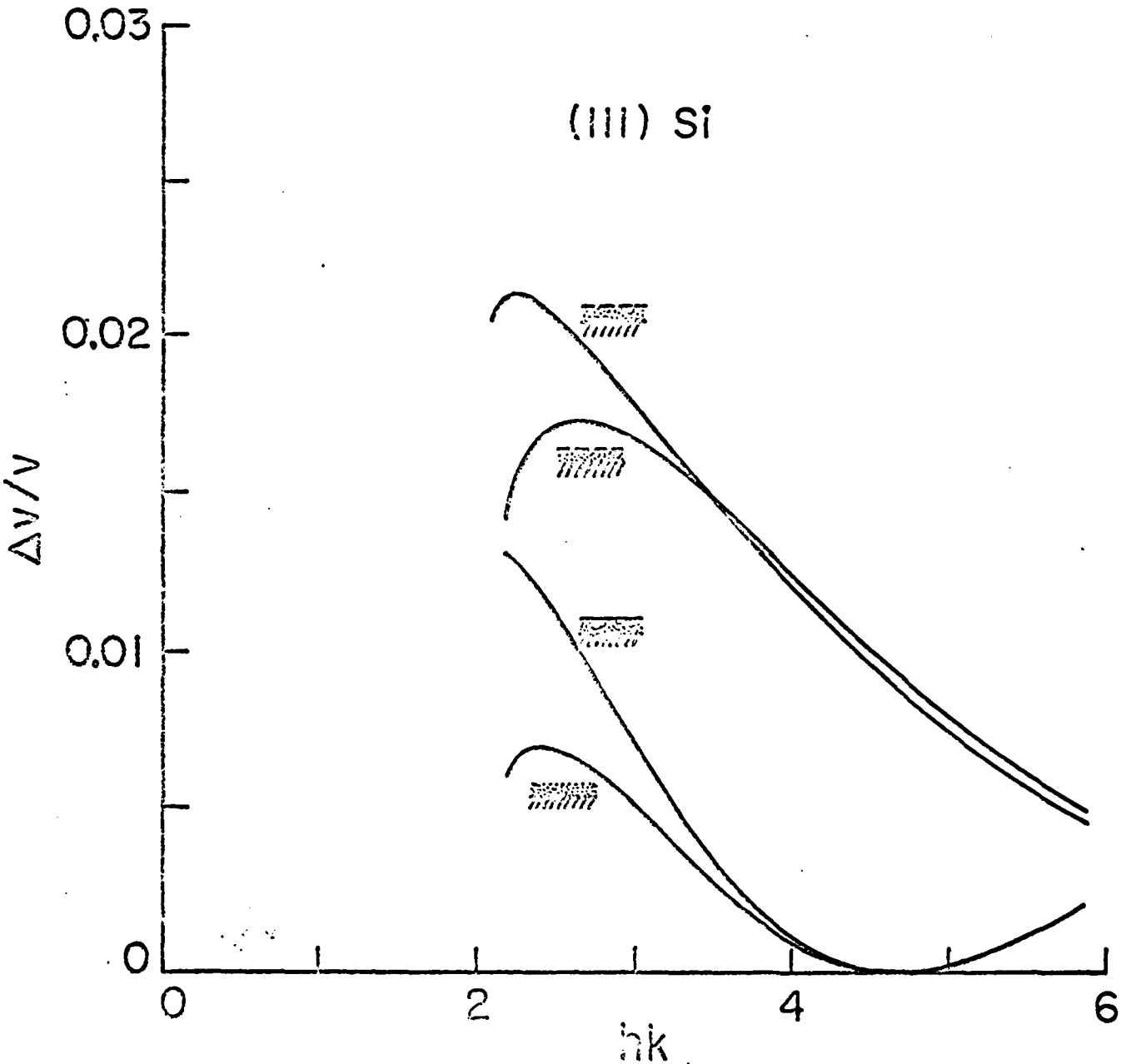
(111) Si
0.03
0.02
0.01
0
Δv/v
0
2
4
6
hk

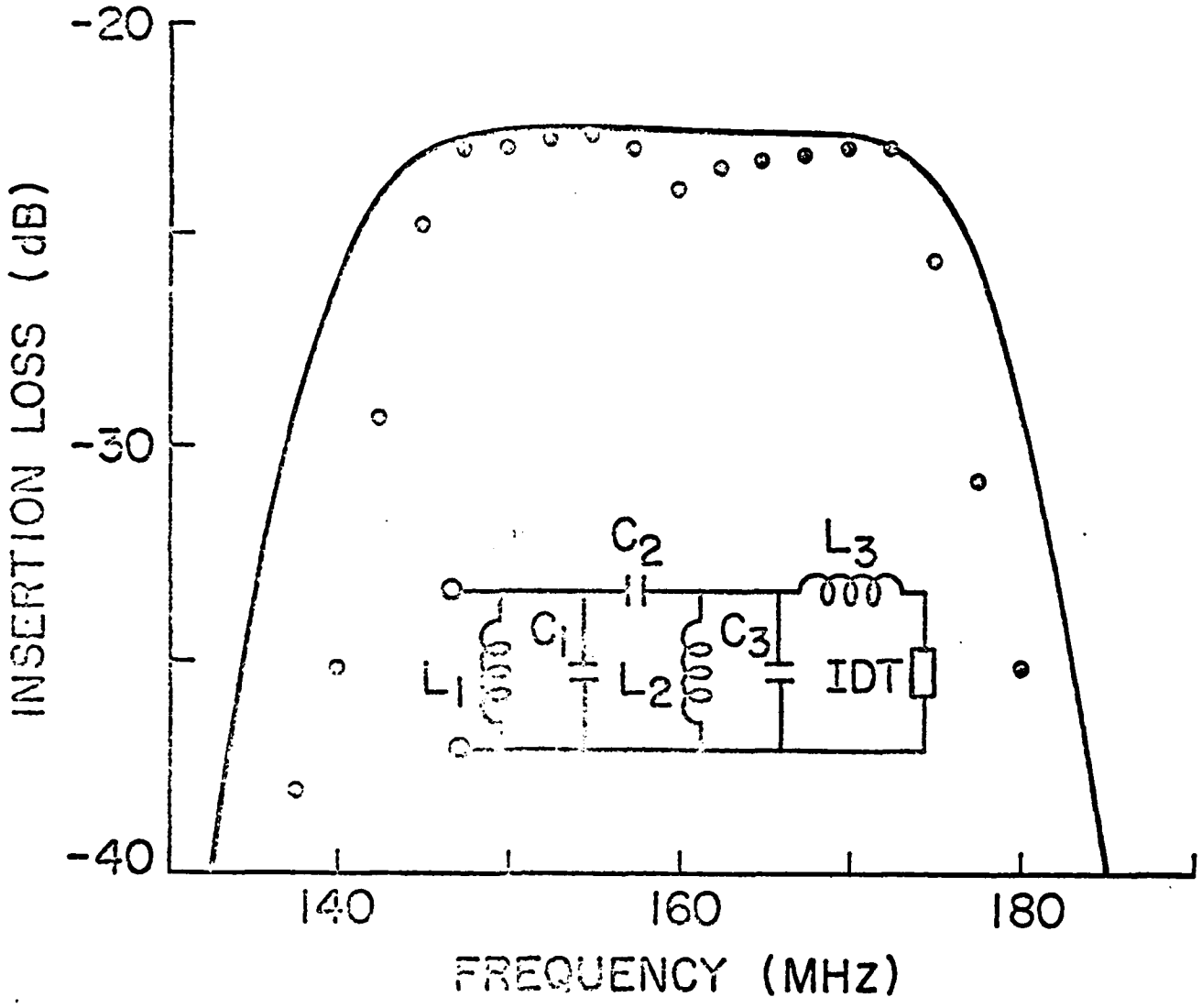
-20
-30
-40
INSERTION LOSS (dB)
140
160
180
FREQUENCY (MHz)
C2
L3
C1
C3
L1
L2
IDT

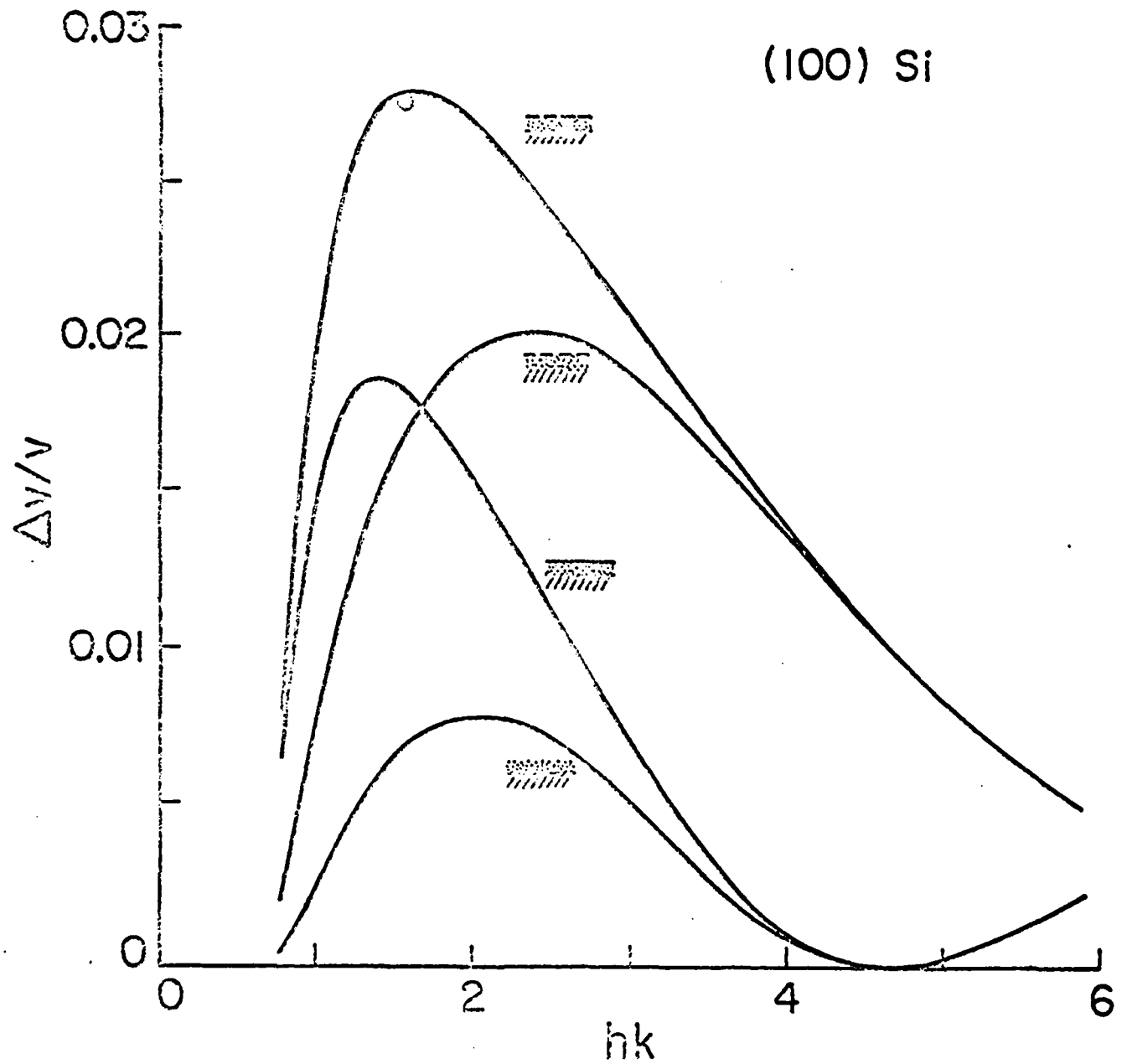
(100) Si
0.03
0.02
0.01
0
Δv/v
0
2
4
6
hk

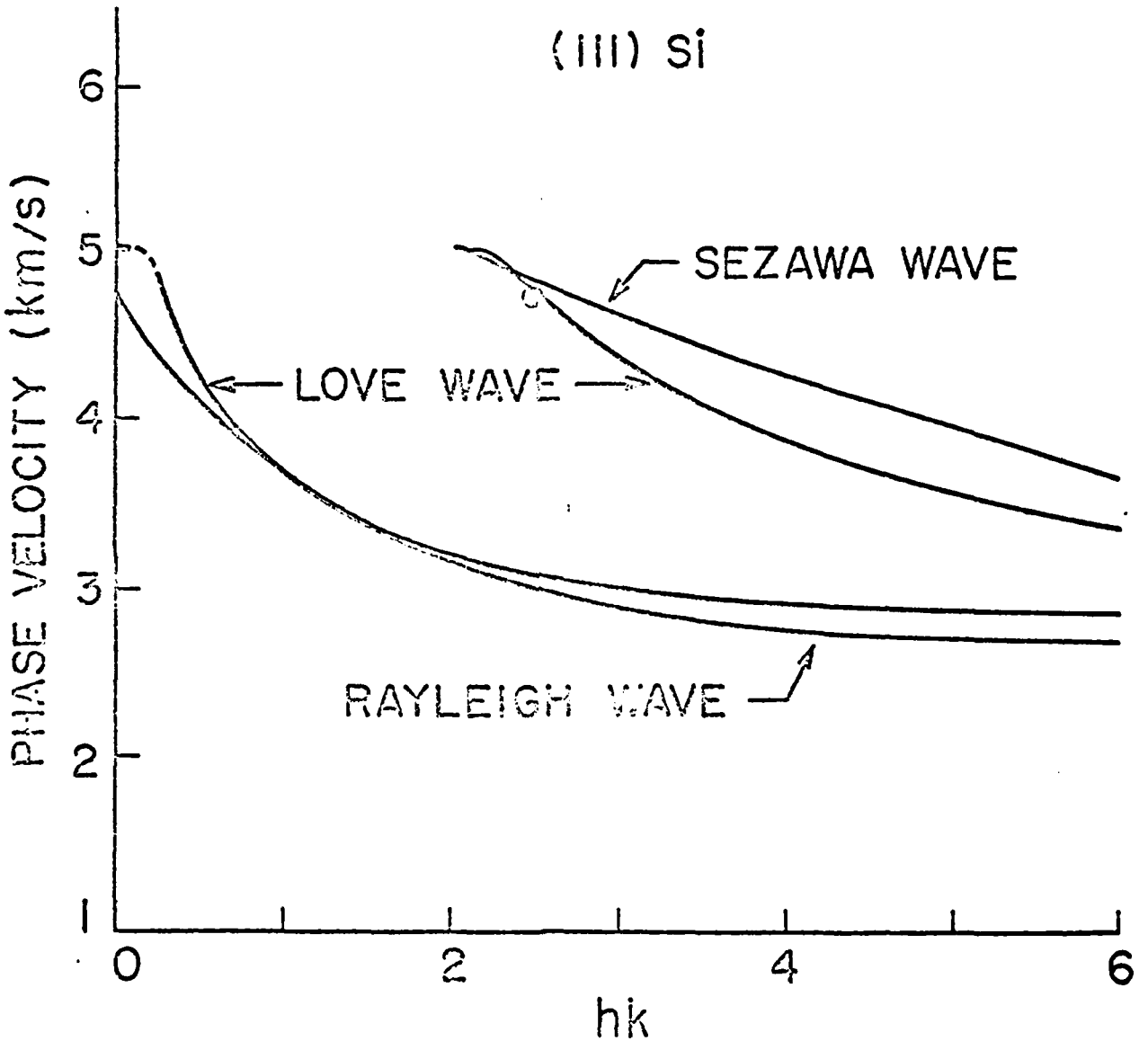
(111) Si
PHASE VELOCITY (km/s)
SEZAWA WAVE
LOVE WAVE
RAYLEIGH WAVE
1
2
3
4
5
6
0
2
4
6
hk

APPENDIX II

ADAPTIVE DECONVOLUTION USING AN ASW STORAGE CORRELATOR

J. E. Bowers, G. S. Kino, D. Behar, and H. Olaisen

Ginzton Laboratory
Stanford University
Stanford, California

Abstract

A new analog adaptive filter for deconvolving distorted signals is described in this paper. The filter uses a storage correlator which implements a clipped version of the LMS algorithm and uses a special iterative technique to achieve a fast convergence. The new filter has a potential bandwidth of 100 MHz and would eventually handle pulsed signals of 5 μsec width. For signals with time-bandwidth product of less than 100, the adaptation time is less than 1 msec which allows operation in real time for most applications including resolution of radar signals in a cluttered environment, removal of echoes from television signals, deconvolution of distorted signals in nondestructive evaluation, and also in telephony. The filter is particularly suited for radar and communications as it processes signals directly in the VHF range.

Two experiments related to ghost suppression of a pulse and to the field of NDE are described in this paper. The results are in good agreement with computer simulations and show a ghost suppression of 15 dB for the first example and a sidelobe suppression of 8 dB for a transducer signal. The adaptation time is less than 450 μsec.

I. INTRODUCTION

Adaptive filtering[1] is useful in removing distortion from signals, particularly when the distortion varies in time. Adaptive filters have been used to perform deconvolution of a distorted echo pulse in an acoustic imaging system[2], to equalize the distortion in a telephone channel[3], and to suppress an interfering signal[4].

Most adaptive filters have been implemented using digital techniques. The limitation of the digital approach is the limited bandwidth (typically 5 MHz) and the practical limit on the number of taps dictated by the complexity and power consumption[5].

An analog-digital hybrid approach has been implemented using MOS LSI technology[6]. This has the advantage of lowering the power consumption and allowing 32 taps to be used without undue external complexity. Large dynamic range was obtained with this technique (60 dB), but the bandwidth was limited to less than 1 MHz.

Most analog implementations of an adaptive filter have been made using CCDs with analog tap weights held in sample and hold circuits[7]. The limitations here are the narrow bandwidth and variation across the chip in gain and threshold levels. The alternative approach used at Hughes for implementing a wideband adapting filter is to employ tapped ASW filters with complex computer-controlled systems for adjusting the tap weights[8].

We shall describe here a relatively simple all-analog approach to adaptive filtering which uses the least mean squares (LMS) algorithm to find the optimal set of tap weights. An ASW monolithic ZnO/Si storage correlator with 8 MHz bandwidth and the equivalent of 24 taps was used[9]. The advantages of this approach are:

(1) fast iteration rate (100 kHz) which means a short learning time (~100 μs) and good ability to track time varying signals;

(2) simple external connections;

(3) large potential bandwidth (100 MHz);

(4) large potential number of taps (1000);

(5) low power consumption (.1 W);

(6) it is suited for radar and communications systems because it can operate directly at the IF frequency.

A disadvantage is that, at the present time, the dynamic range is less than for digital systems.

A brief introduction to the LMS algorithm is provided, followed by a new derivation of the LMS algorithm. As the class of applications discussed here utilizes continuous, quasistatic filters, a derivation in the frequency domain rather than the time domain allows more physical insight into the processing capability of the LMS algorithm and into its advantages and limitations for these kinds of applications.

Two adaptive deconvolution experiments which used the storage correlator are described. In the first experiment, an undesirable time-delayed ghost pulse is removed. In the second experiment, the ringing in the pulse response of an acoustic transducer is removed by adaptive filtering. The results of these experiments are compared to computer simulations with the LMS algorithm. Conclusions are drawn regarding which properties and nonlinearities of the storage correlator are limiting the performance of the adaptive filter.

II. EXPERIMENTAL PROCEDURE

A. The LMS Algorithm

Consider an adaptive filter with an input $x(t)$ and output $y(t) = x * w$. The tap weights w are adjusted after each iteration such that the output $y(t)$ converges to a desired signal $d(t)$. The time it takes for convergence to occur is commonly called the learning or training time. After the optimum set of weights w is determined, the filter can be used to remove the distortions in signals. For example, in a TV system with a ghost, the filter can be trained on the sync signal (which occurs at the end of each line) to remove the echo sync signal, and then the entire TV line can be passed through the filter, and the "ghosts" will be removed.

The error $\varepsilon(t)$ between the desired signal $d(t)$ and the output of the filter $y(t)$ is

$$\varepsilon(t) = d(t) - y(t) \tag{1}$$

where

$$y = x * w \tag{2}$$

and $*$ indicates convolution. Then the LMS algorithm specifies that to minimize the error, w must be changed by Δw such that

$$\Delta w = \mu x \star \varepsilon \tag{3}$$

where $\star$ indicates correlation and μ is a constant which determines the rate of convergence of the system.

Thus it follows from Eqs. (1), (2), and (3) that

$$\Delta w = \mu x \overset{*}{\times} (d - x * w) \qquad (4)$$

A proof is given in the following section that if these adjustments Δw are made, then the weights exponentially approach the Wiener filter solution; this is a filter which minimizes the average mean square error, over the frequency band of interest, between its output signal and a desired signal $D(\omega)$.

It can be seen from the expression for the tap weight adjustment (Eq. (4)) that for each iteration, a convolution with x , and a correlation with x must be performed. In addition, an analog storage register is needed for w , and it must be possible to adjust each of the tap weights.

The ASW storage correlator is ideally suited for this purpose, as it can perform all of these operations (convolution, correlation, addition, and storage). A big advantage of this approach is its simplicity. All of the necessary operations are performed inside a two (or three) port device in real time.

B. The Storage Correlator

The ASW storage correlator is a device which utlizes the interaction between a propagating acoustic surface wave and a charge distribution stored in an array of diodes to store, correlate, or convolve two broad bandwidth signals in real time. A series of signals may be added together by successively storing them in the diode array. A brief description of the storage correlator follows. Complete descriptions of the device[10,11] and its operation [12] as well as a theory of the device[13] are given in the literature.

A schematic drawing of a storate correlator is shown in Fig. 1. If a modulated carrier x is applied to the acoustic port (#2) and a signal ϵ to port #3 , then the charge distribution[13]

$$\Delta w = x \star \epsilon \tag{5}$$

is added to the charge distribution w stored in the diode array. If a signal x is then applied to port #3, then the convolution

$$y = x * w \tag{6}$$

is the output at port #2. The LMS algorithm can be realized by repeating the process many times. Eventually, the tap weights w converge to an approximation to the Wiener solution, and the programming is complete. The filter may then be used to deconvolve other signals which have been distorted in the same manner.

The external connections used to operate the storage correlator are indicated in Fig. 2a. A much simpler method is indicated in Fig. 2b when two acoustic ports of the correlator are used, and the external delay line and the switches are not needed. A difference amplifier is not needed to subtract $d(t)$ and $y(t)$; rather the carrier frequency is adjusted so that there was a phase difference of π between the delayed signal $y(t)$ and the desired signal $d(t)$. This is explained more fully in the next section.

The storage correlator is not an exact implementation of the Widrow type LMS adaptive filter for two reasons. First, the LMS algorithm requires that each tap be changed individually and the error signal for

the next tap be calculated after the previous tap is changed[14]. However, in our implementation, the entire error signal is calculated, and the entire set of taps is changed at once. This difference is not significant except for the case of very high gain and very fast convergence. The second difference is that the effect of the plate signal (port #3) on the tap weights is not linear (Fig. 3). If the error signal is less than a threshold determined by the characteristics of the devices (4V), the tap weights are unaffected. The error signal is clipped around 9V, so only ~6 dB of dynamic range is available at port #3. If the error signal is fed into an acoustic port (as in Fig. 4b), then at least 35 dB dynamic range should be available.

The weight signal $w(z)$ is stored in 2000 diodes; however, the number of equivalent taps is much less since the bandwidth is 8 MHz and the maximum signal duration is 3 μs. Consequently, the time bandwidth product is 24. The device was represented in the computer simulation by a 24 tap transversal filter. The necessary correlations and convolutions were calculated in the computer, and the error signal was modified according to the transfer characteristic shown in Fig. 3. It can be seen that this transfer characteristic closely approximates the experimentally observed characteristic.

III. THEORY

A. Introduction

The LMS algorithm has been analyzed in detail by Widrow[14,15]. The first task in his analysis is to transform from the coordinate system consisting of N samples from the waveform to a set of normal coordinates where the correlation matrix is diagonal; the eigenvectors of the correlation matrix are mutually orthogonal, and, most importantly,

the decay modes are uncoupled. Once this transformation is accomplished, expressions for the decay constants τ_p, misadjustment, etc. may be derived.

In the analysis presented here, the transformation is very easily accomplished by taking the Fourier transform of all quantities. Correlations are then simple products, and the convergence of a quantity at a given frequency is independent of other frequencies, i.e., the modes are uncoupled.

B. Convergence

Consider the situation in Fig. 2, where all signals are rf modulated, and the carrier frequency is ω_0. The desired signal $d_n(t)$ and the distorted signal $x_n(t)$ are repetitive, and as the number of iterations n increases, the only change in these signals is a phase change

$$d_n(t) = d(t)\, e^{j\omega_0 nT} \tag{7}$$

where T is the iteration time. In the frequency domain

$$D_n(\omega) = D(\omega)\, e^{j\omega_0 nT} \tag{8}$$

Similar expressions hold for the distorted signal $X(\omega)$.

The filter output is

$$Y_n(\omega) = X(\omega) W_n(\omega)\, e^{j\omega_0 (nT + T_0)} \tag{9}$$

and the error signal is

$$E_n(\omega) = D_n(\omega) + Y_n(\omega)\, e^{-j\omega_0 T_D}$$

$$= D(\omega)\, e^{j\omega_0 nT} + X(\omega) W_n(\omega)\, e^{j\omega_0 (nT + T_0 - T_D)} \tag{10}$$

where T_D is the length of the external delay line, and T_0 is the time between the appearance of $x(t)$ at the acoustic and plate ports.

The weight adjustment is

$$w(t) = 2\mu_a X(t) \star \varepsilon_n(t) \tag{11}$$

Equivalently, we can write

$$W_{n+1}(\omega) = W_n(\omega) + 2\mu E_n(\omega) X_n^*(\omega)$$

$$W_{n+1}(\omega) = A W_n(\omega) + B \tag{12}$$

where

$$A = 1 + 2\mu X(\omega) X^*(\omega)\, e^{j\omega_0 (T_0 - T_D)}$$

$$B = 2\mu D(\omega) X^*(\omega) \tag{13}$$

Equation (12) has the solution

$$W_n(\omega) = (W_i - W_w) A^n + W_w \tag{14}$$

where W_i is the initial weight distribution and

$$W_w = \frac{D(\omega)}{X(\omega)} e^{j\omega_0(T_0 - T_D)} \tag{15}$$

Equation (14) converges only if $|A| < 1$. The fastest convergence is obtained for the carrier frequencies where the error signal is the subtraction of D and Y, i.e. when

$$\omega_0 = \frac{\pi}{|T_D - T_0|}(2p + 1) \tag{16}$$

where p is a large integer. If the feedback gain μ is sufficiently small

$$\mu < \frac{1}{XX^*} \tag{17}$$

hen the convergence requirement $|A| < 1$ is satisfied for carrier frequencies in bands of width $\Delta\omega$ around the frequencies given by Equation (16), where

$$\Delta\omega = \frac{2}{|T_D - T_0|} \arccos(\mu XX^*) \tag{18}$$

It can be seen from Equation (17) that when μ is near its upper limit, the carrier frequency must be close to one of the values given by Equation (16).

If the feedback gain is significantly less than its maximum value, it follows that

$$A = 1 + 2\mu XX^* e^{j\omega_0(T_0 - T_D)} \approx e^{-1/\tau} \tag{19}$$

where

$$1/\tau = 2\mu XX^* e^{j[\omega_0(T_0 - T_D) + \pi]} \tag{20}$$

The convergence of the weight vector (Eq. (14)) is approximately exponential. So we can write

$$W_n \approx (W_1 - W_w) e^{-n/\tau} + W_w \tag{21}$$

The error is

$$E_n = D - X^*W_n$$

$$E_n \approx X^*(W_i - W_w) e^{-n/\tau} \tag{22}$$

The error decays exponentially to zero. In practice, the bandwidth of the system is limited by the bandwidth B of the acoustic transducers. Consequently, the error outside this frequency range is not affected by the adaptation process. It will also be noted that phase distortion in the system is cancelled out by the application of the convolution and correlation process in turn. So, although this is basically a feedback system, there is no problem with instability provided the convergence criteria are satisfied.

We have implicitly assumed that the signals $x(t)$ and $d(t)$ are sufficiently short compared to the time length of the diode array that all of the signal $\Delta\omega(t)$ is stored in the diode array. If this is not

the case, then different frequencies do not decay independently, and the analysis is more difficult. An important result of this more difficult case is that the error does not decay to zero in the passband.

If noise on the input signal X is included in this analysis, and if the noise on the plate and acoustic ports are correlated, as they would be if a delay line were used to generate the second X signal which is needed during each iteration, then the expression for the convergence of the weight signal is again given by Equation (22) where

$$W_w = \frac{DX^*}{XX^* + \langle NN^* \rangle} \tag{23}$$

$$\tau = \frac{1}{2\mu(XX^* + \langle NN^* \rangle)} \tag{24}$$

Equation (23) is, of course, the Wiener filter solution.

IV. RESULTS AND DISCUSSION

A. Echo Suppression

In this experiment, a square pulse 0.4 μs long is followed by an echo pulse. The desired signal is a single pulse 0.4 μs long. For an echo which is 6 dB less in amplitude than the main pulse (Fig. 4a), the sidelobe suppression after 10 iterations (200 μs) is 15 dB, as shown in Fig. 4b. The dependence of sidelobe suppression on echo height is shown in Fig. 5. The results of computer simulations of the LMS algorithm with 22 taps and using clipping and a threshold 6 dB below the clipping level are also shown in Fig. 5. The computer simulation agrees very well with experimental results except that the maximum sidelobe suppression is 23.5 dB which is 4.5 dB higher than was experimentally

obtained. The reason is that the spurious signals generated in the device during read out limits the dynamic range of the signal input.

An important result obtained in this experiment is that spurious acoustic signals generated by the plate readout signal can be suppressed by up to 13 dB as a result of the adapting process. The filter does not distinguish between echoes and distortions generated externally or by the device itself. This result is demonstrated in Fig. 6. The upper trace is the adaptive filter result after removing an echo from a 0.4 μs long pulse. If all signals except the plate readout signal are removed, the filter output (lower trace) is the spurious signal generated by the plate signal. A large spurious signal can be seen when previously there had been a null.

The advantage of computer simulation of this adaptive filter is that the threshold and clipping levels may be easily changed to see what effect they have on the performance of the adaptive filter. These results are summarized in Table I. The computer simulated linear LMS result is given in the first row. If a threshold level is included, then the computer simulation converges much faster, but to worse results. The values obtained are in agreement with experimental results. If the feedback gain is increased so that the error signal is now clipped, then much better sidelobe suppression is obtained in both the experimental and computer simulation cases. We note that clipping of the signal increases the rate of convergence radically, as has been noted by others. The algorithm employed is therefore known as the clipped LMS algorithm.

Regardless of the shape of the desired signal (d) and input signal (x), it was <u>always</u> experimentally observed that the feedback gain must be large enough to strongly clip the error signal during the first few iterations for the optimum filtering. After many iterations, the error signal is only slightly clipped.

The threshold and clipping levels can be changed by modifying the design of the storage correlator. For this reason, a series of computer simulations was made to determine the effect of having other threshold to clipping ratios (σ) than the value $\sigma = .5$ which exists in the present devices. Only the ratio σ is important here. The minimum r.m.s. error does not change if the threshold, clipping, and gain values are all multiplied by the same value. The asymptotic value of the r.m.s. error is shown as a function of σ in Fig. 7 for the case of a 6 dB echo. The optimum value for the gain is used at each point. The end point $\sigma = 1.0$ corresponds to the situation of hard clipping where the threshold level equals the clipping level, and the feedback error is either 1 or 0. The r.m.s. error increases linearly with σ. This is intuitively expected since any error values less than the threshold do not affect the tap weights and are not adapted to zero. The r.m.s. error would then linearly increase with threshold level. Consequently, the design of the storage correlator should minimize the threshold value.

B. Reduction of Bulk Transducer Ringing

The object of this experiment was to improve the impulse response of an acoustic bulk wave 1.25 Mlz transducer used for acoustic nondestructive evaluation. The impulse response is shown in Fig. 8a. The desired signal is a unipolar pulse with a width of .3 μs. If the impulse response is correlated with itself (Fig. 8b), the highest sidelobe is 1.7 dB smaller than the peak. However, if the correlator is used as an adaptive filter, then the sidelobe level can be reduced to 7 dB below the peak after 10 iterations (Fig. 8c) and 10 dB below the peak after 35 iterations.

The growth of the peak as the number of iterations increases is shown in Fig. 9. The computer simulation is also shown and can be seen to be in good agreement with the experimental result. The computer

simulation is in good agreement with the experimental result except that the maximum predicted suppression is 2.6 dB better than was experimentally observed.

Linear LMS theory predicts[1] that the time averaged mean square error (MSE) should decay exponentially to a constant value. The ratio of this constant value to the Wiener solution is called the misadjustment M . The misadjustment is approximately related to the decay constant τ by the relation[1]

$$M = N/4\tau \qquad (25)$$

where N is the number of tap weights. In our case, N is the time bandwidth product of the storage correlator. Thus, the faster the convergence, the larger the misadjustment.

The experimentally observed decay of the MSE for the bulk transducer case is shown in Fig. 9. The decay is exponential except for the first few iterations when the error signal is strongly clipped and the mean square error decays faster than an exponential. The experimental decay constant is 7.5, and the misadjustment calculated from Equation (25) is equal to .8 . We interpret this to mean that the final result is close to the Wiener solution.

C. Limitations

The bandwidth of this device (8 MHz) is larger than the bandwidth of other methods of implementing the LMS algorithm; however, larger bandwidths are often desirable. Our technique can work well as an adaptive filter for a 1.25 MHz transducer, but it works poorly for a 2.5 MHz transducer. The diode array length (3 μs) is also a limitation since we cannot

adapt signals which are longer than this. Also, since the correlation signal is truncated, the filter output is distorted. These two limitations are manifestations of the fact that if the correlator had a larger time bandwidth product than 24, then it would equivalently have more taps and could adapt a broader class of signals. Time bandwidth products of 500 or more are possible with the use of present technology. Note, however, that Equation (25) predicts that if the number of taps is increased, then the convergence time also increases (for a given level of misadjustment). Thus, a larger number of taps is not desirable for applications in which the distortion is changing rapidly. For example, if the timing or amplitude of the echo significantly changes over a time period of 200 μs (10 iterations), then a larger number of taps would not be desirable.

V. CONCLUSIONS

It was demonstrated that a -6 dB echo could be suppresed to -15 dB in 200 μs (10 iterations). The sidelobe of the impulse response of a 1.25 MHz acoustic bulk transducer can be reduced from -2 dB to -10 dB with adaptive filtering.

The experimental results are on the whole in excellent agreement with the computer simulations. Thus it appears that the storage correlator is being operated in the optimum manner and that the only major distortion introduced by the storage correlator is the presence of the threshold and clipping levels.

There are many advantages of using a storage correlator to implement the clipped LMS algorithm for adaptive filtering. Only two connections are needed for a device which can correlate, convolve, store, and add

broadband rf signals in real time. The device is small (1 cm^2) and has the potential of much broader bandwidths (100 MHz) than is obtainable with digital techniques. The device is far faster in operation than any competitive inverse filter with its bandwidth.

ACKNOWLEDGMENT

The authors wish to thank C. Williams, B. T. Khuri-Yakub, and H. Tuan for valuable discussions and suggestions. This work was supported by the Defense Advance Research Projects Agency and monitored by the Office of Naval Research under Contract N00014-76-C-0129.

REFERENCES

1. J. M. McCool and B. Widrow, "Principles and Applications of Adaptive Filters," IEE Conf. Publ., 144, pp. 84-95, 1976.
2. D. Corl, "A C.T.D. Adaptive Inverse Filter," Electr. Lett., 14, pp. 60-62, 1978.
3. R. W. Lucky, "Automatic Equalization for Digital Communications," Bell Sys. Tech. J., 66, pp. 547-588, 1965.
4. P. M. Grant and G. S. Kino, "Adaptive Filter Based on SAW Monolithic Storage Correlators," Electr. Lett., 14, pp. 562-564, 1978.
5. D. Behar, et al., "The Use of a Programmable Filter for Inverse Filtering," submitted for publication, Electr. Lett., October 1979.
6. B. K. Ahuja, et al., "A Sampled Analog MOS LSI Adaptive Filter," IEEE J. Solid-State Cir., SC-14, pp. 148-154, 1979.
7. D. F. Barbe, et al., "Signal Processing with Charge Coupled Devices," IEEE J. Solid-State Cir., SC-13, pp. 34-51, 1978.
8. W. K. Masenten, "Adaptive Processing for Spread Spectrum Communications Systems," Report TP 77-14-22, Hughes Aircraft Co., September 1977.
9. D. Behar, et al., "The Storage Correlator as an Adaptive Inverse Filter," submitted for publication, Appl. Phys. Lett., December 1979.
10. K. A. Ingebritsen, et al., "A Scottky-Diode Acoustic Memory and Correlator," Appl. Phys. Lett., 26, pp. 596-598, 1975.
11. C. Maerfeld and Ph. Defranould, "A Surface Wave Memory Device Using pn Diodes," IEEE Ultrasonics Symp. Proc., pp. 209-211, 1975.
12. H. C. Tuan, et al., "A New Zinc Oxide-on-Silicon Monolithic Storage Correlator," IEEE Ultrasonics Symp. Proc., 496-499, 1977.

13. P. G. Borden and G. S. Kino, "An Analytic Theory for the Storage Correlator," IEEE Ultrasonic Symp. Proc., pp. 485-491, 1977.

14. B. Widrow, et al., "Stationary and Nonstationary Learning Characteristics of the LMS Adaptive Filter," Proc. IEEE, 64, pp. 1151-1162, 1976.

15. B. Widrow and J. M. McCool, "A Comparison of Adaptive Algorithms Based on the Methods of Steepest Descent and Random Search," IEEE Trans. Ant. and Prop., AP-24, pp. 615-637, 1976.

TABLE I

Experimental Results and Computer Simulations for a Filter Input of a .4 μs Wide Pulse with a -6 dB Echo. The Computer Simulation Uses 24 Taps.

	STORAGE CORRELATOR RESULTS		COMPUTER SIMULATION	
	Sidelobe Suppression (dB)	Number of Iterations for Convergence	Sidelobe Suppression (dB)	Number of Iterations for Convergence
Linear	---	---	14.0	25
Threshold*	10.0	5	10.7	4
Threshold and Clipped	14.8	10	14.2	6

*The maximum feedback signal (ε) was not more than 6 dB above the threshold level.

FIGURE LEGENDS

1. Schematic drawing of storage correlator.
2. (a) Actual and (b) proposed implementation of SAW adaptive filter.
3. Correlator output as a function of plate (readout) pulse height.
4. (a) Input signal and (b) output signal after 22 iterations.
5. Experimental and computer simulation results for echo suppression experiment.
6. Echo reduction after 10 iterations (upper trace). Spurious signals generated by plate read-out signal (lower trace).
7. Minimum r.m.s. error as a function of threshold level.
8. (a) Impulse response of 1.25 MHz bulk acoustic transducer; (b) auto-correlation of impulse response; and (c) filter output after 10 iterations of adapting.
9. Output pulse level during adapting process.
10. Mean Square Error during adapting process.

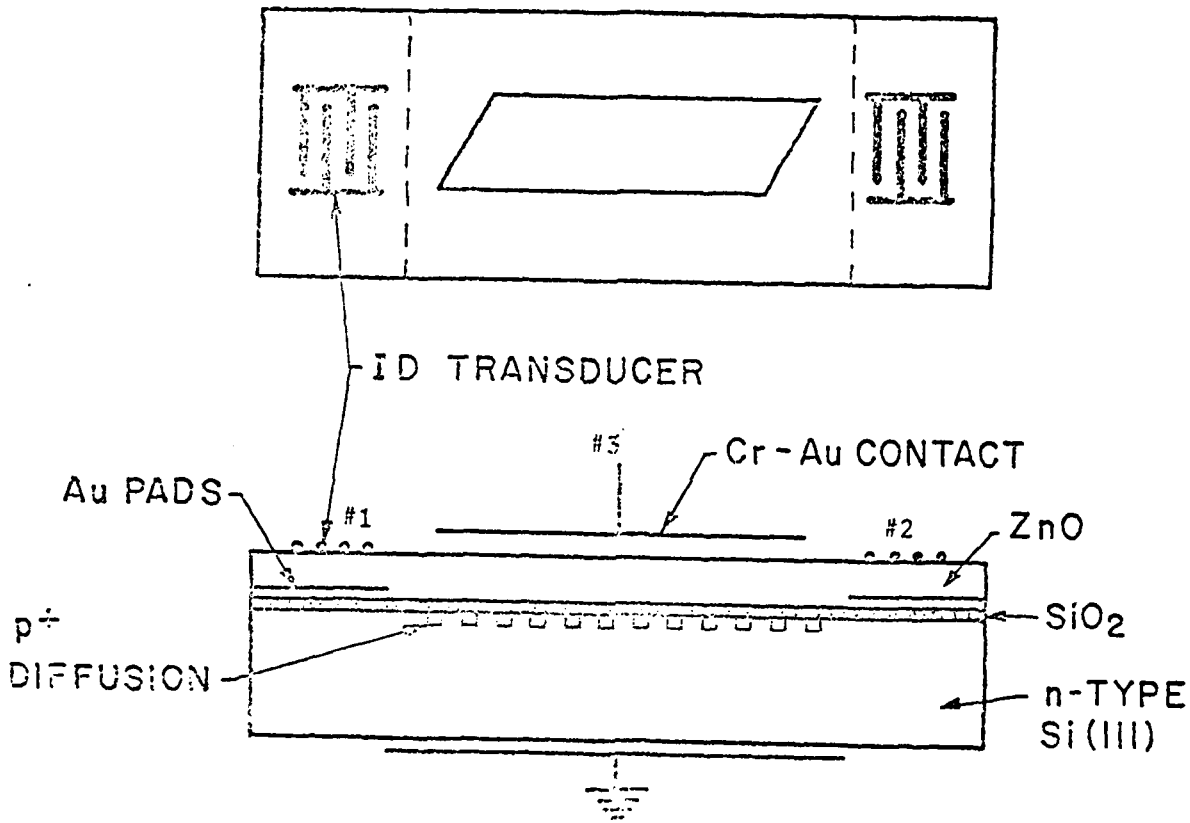
ID TRANSDUCER
#3
Cr-Au CONTACT
Au PADS
#1
#2
ZnO
p+
DIFFUSION
SiO2
n-TYPE
Si(III)

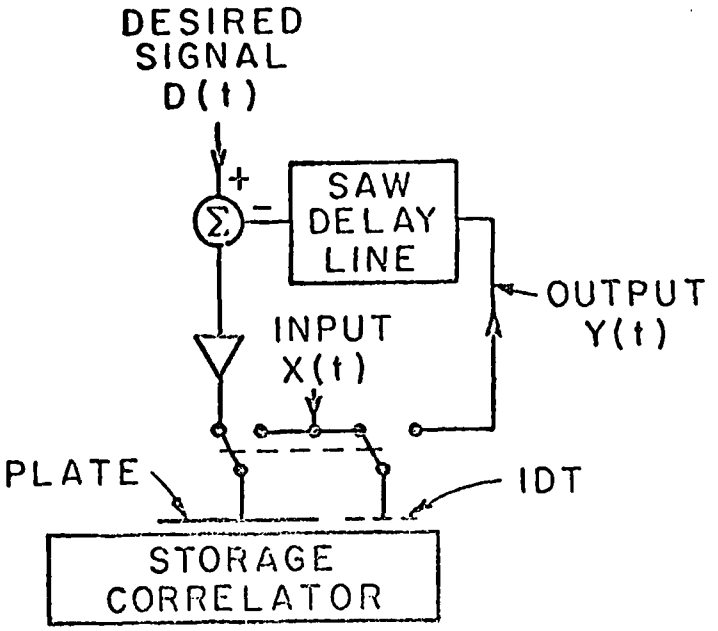
DESIRED
SIGNAL
D(t)
+
Σ
−
SAW
DELAY
LINE
OUTPUT
Y(t)
INPUT
X(t)
PLATE
IDT
STORAGE
CORRELATOR

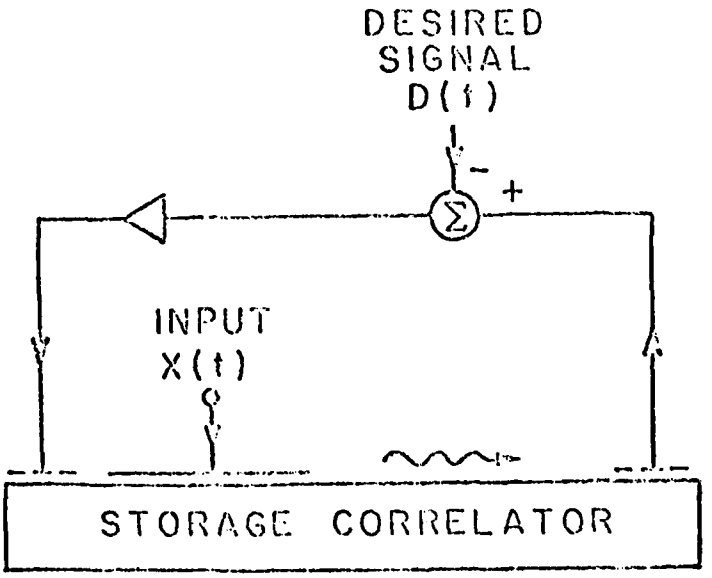
DESIRED
SIGNAL
D(t)
−
+
Σ
INPUT
X(t)
STORAGE CORRELATOR

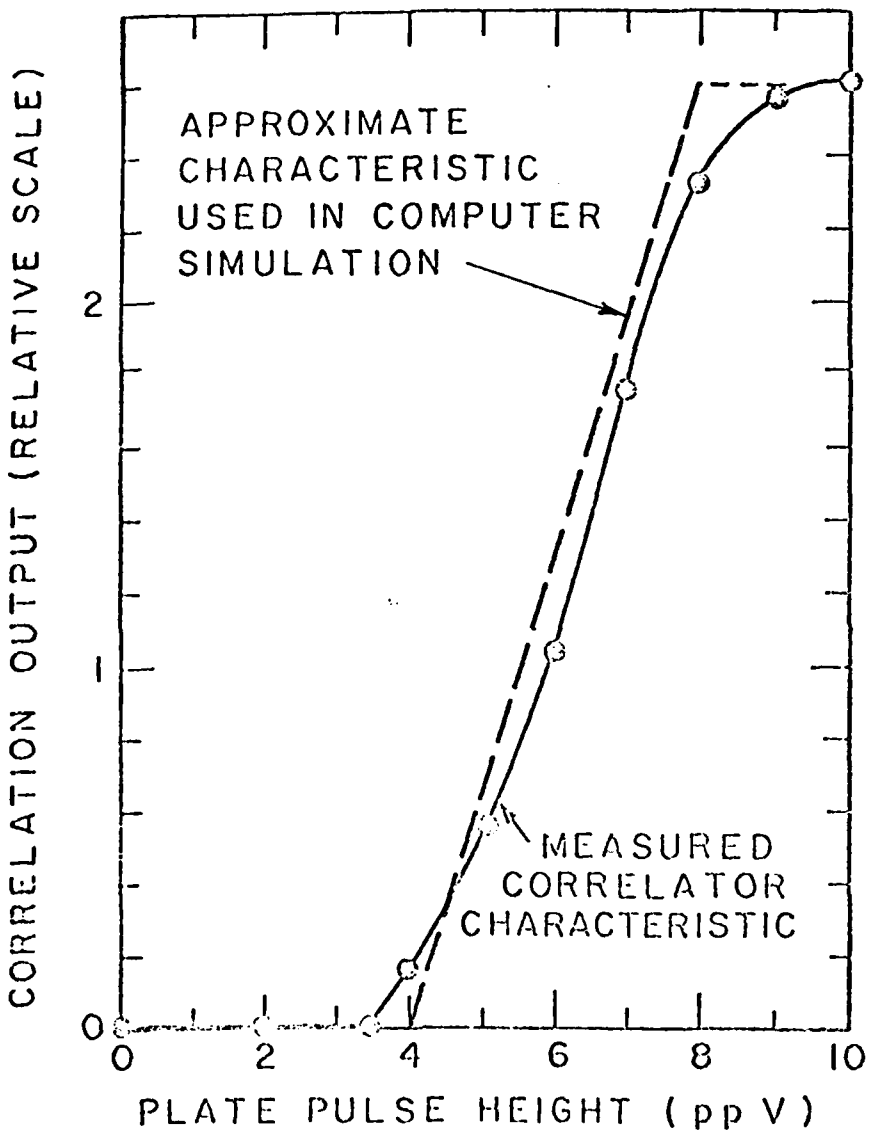
APPROXIMATE
CHARACTERISTIC
USED IN COMPUTER
SIMULATION
MEASURED
CORRELATOR
CHARACTERISTIC
CORRELATION OUTPUT (RELATIVE SCALE)
0
1
2
0
2
4
6
8
10
PLATE PULSE HEIGHT (pp V)

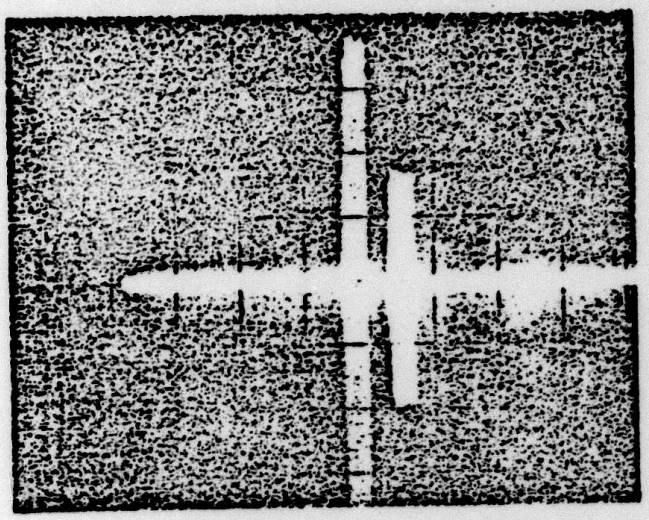

(a) 1 μsec

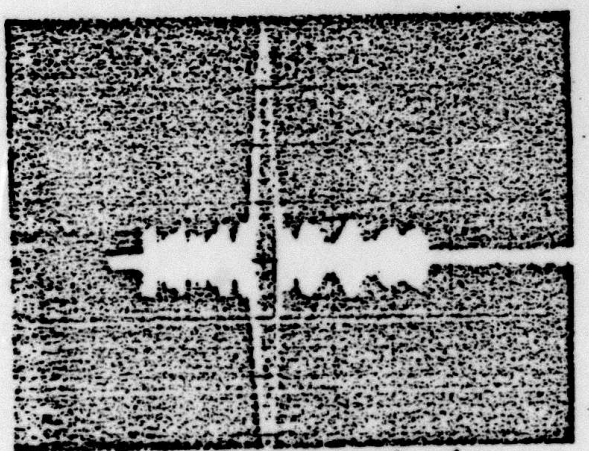

(b) 1 μ sec

Fig. 4.

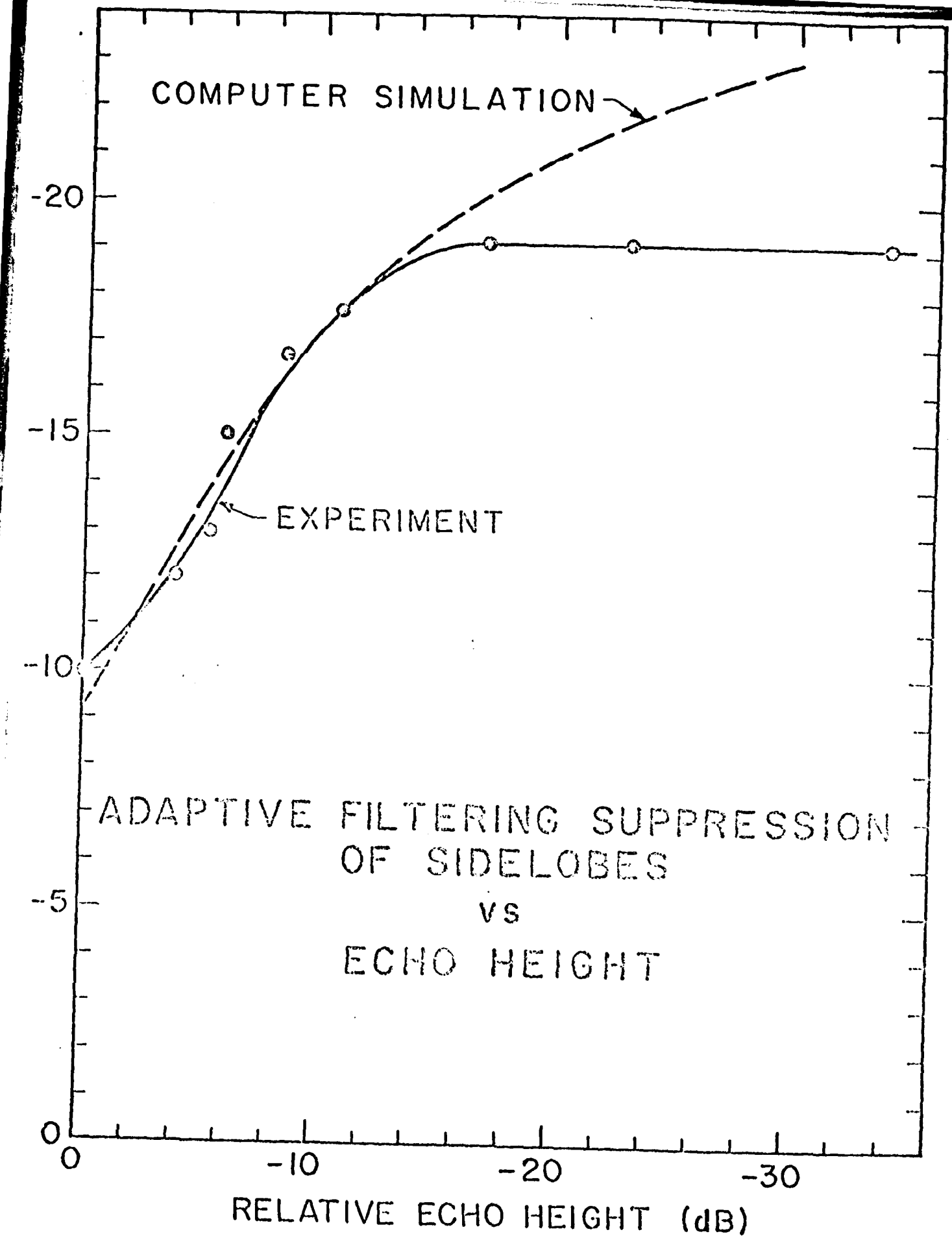
COMPUTER SIMULATION
EXPERIMENT
-20
-15
-10
-5
0
0
-10
-20
-30
ADAPTIVE FILTERING SUPPRESSION
OF SIDELOBES
VS
ECHO HEIGHT
RELATIVE ECHO HEIGHT (dB)

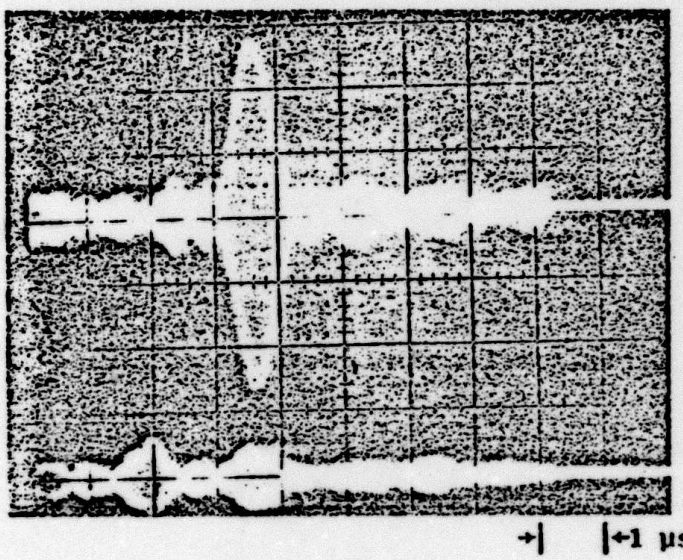

Fig. 6.

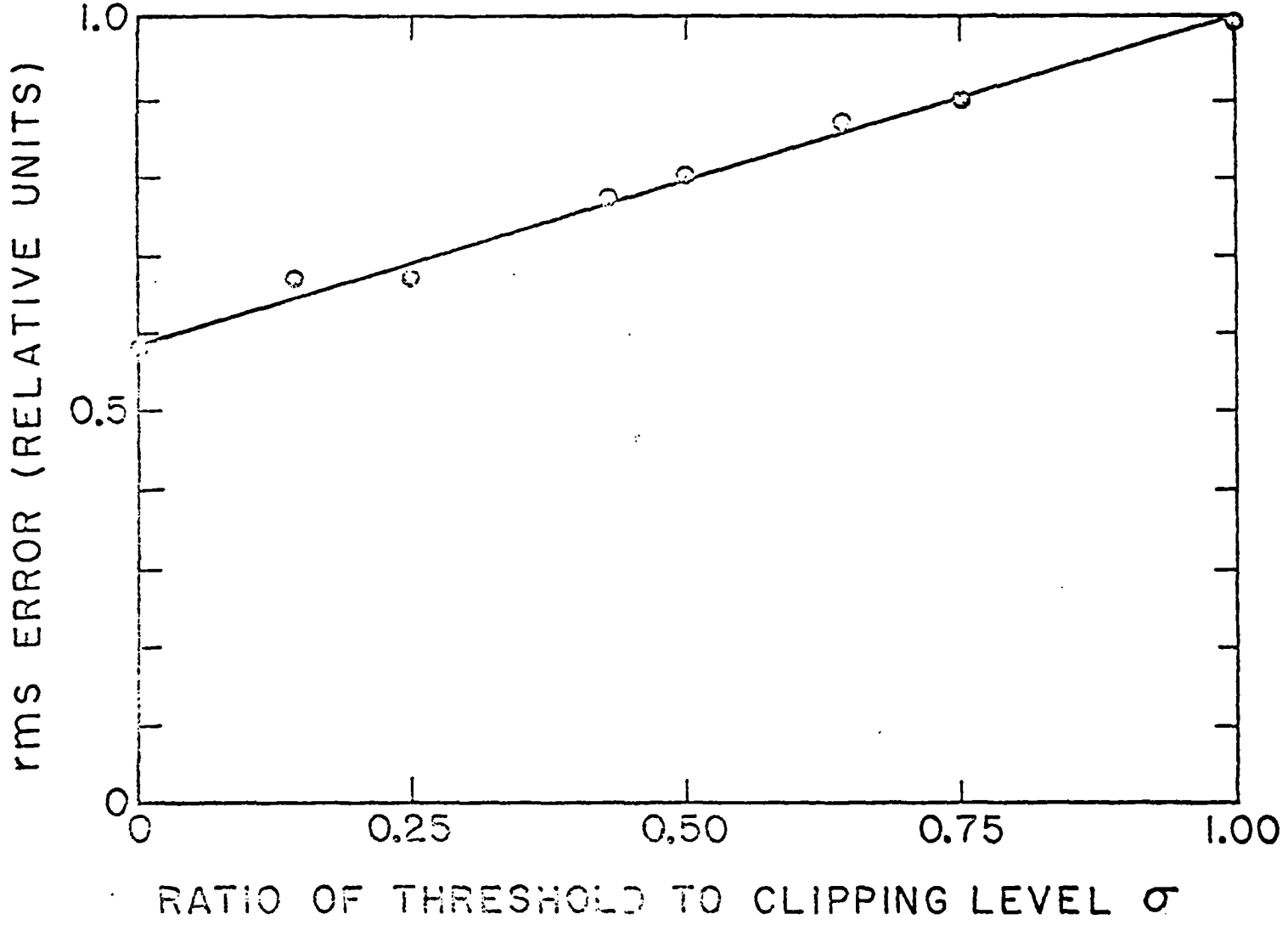
1.0
0.5
0
rms ERROR (RELATIVE UNITS)
0
0.25
0.50
0.75
1.00
RATIO OF THRESHOLD TO CLIPPING LEVEL σ

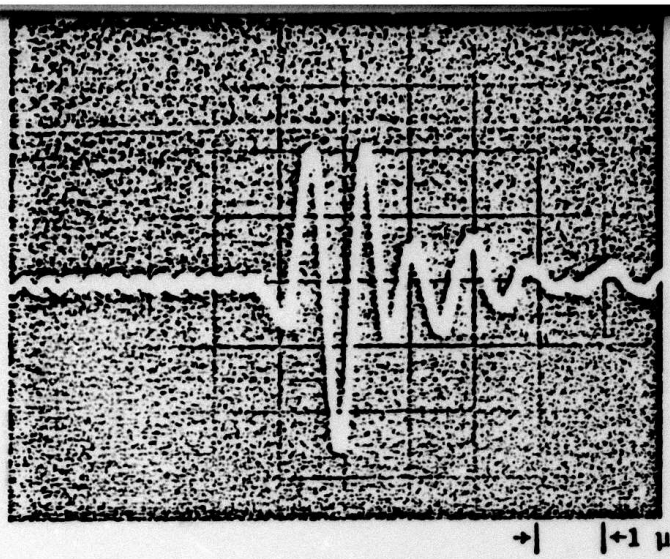

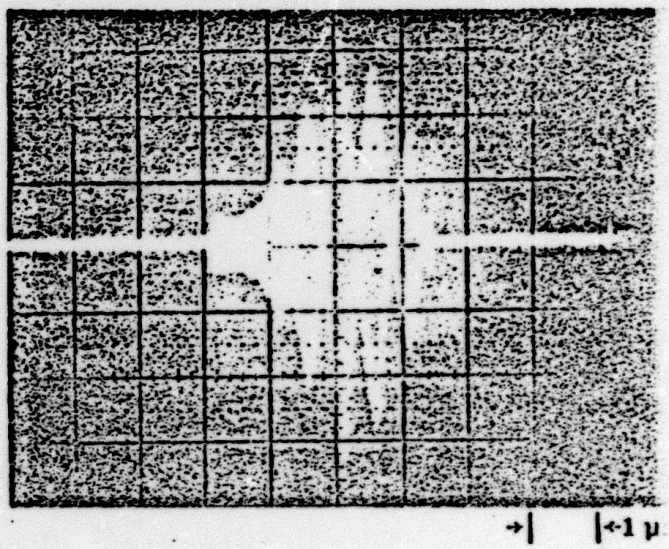

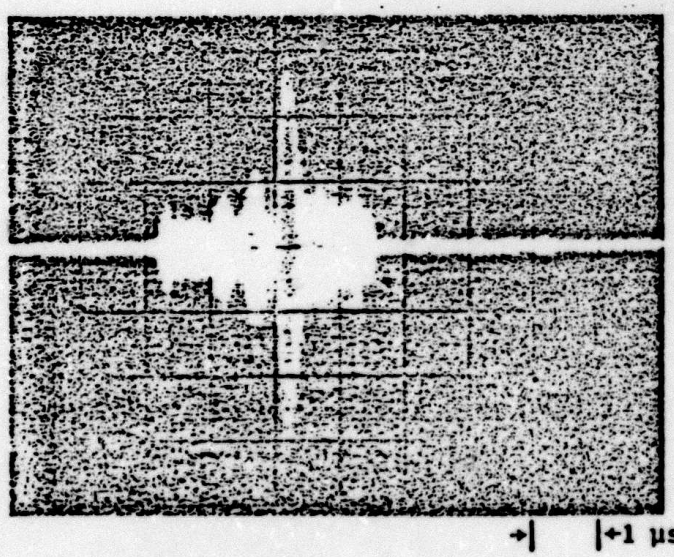

Fig. 8.

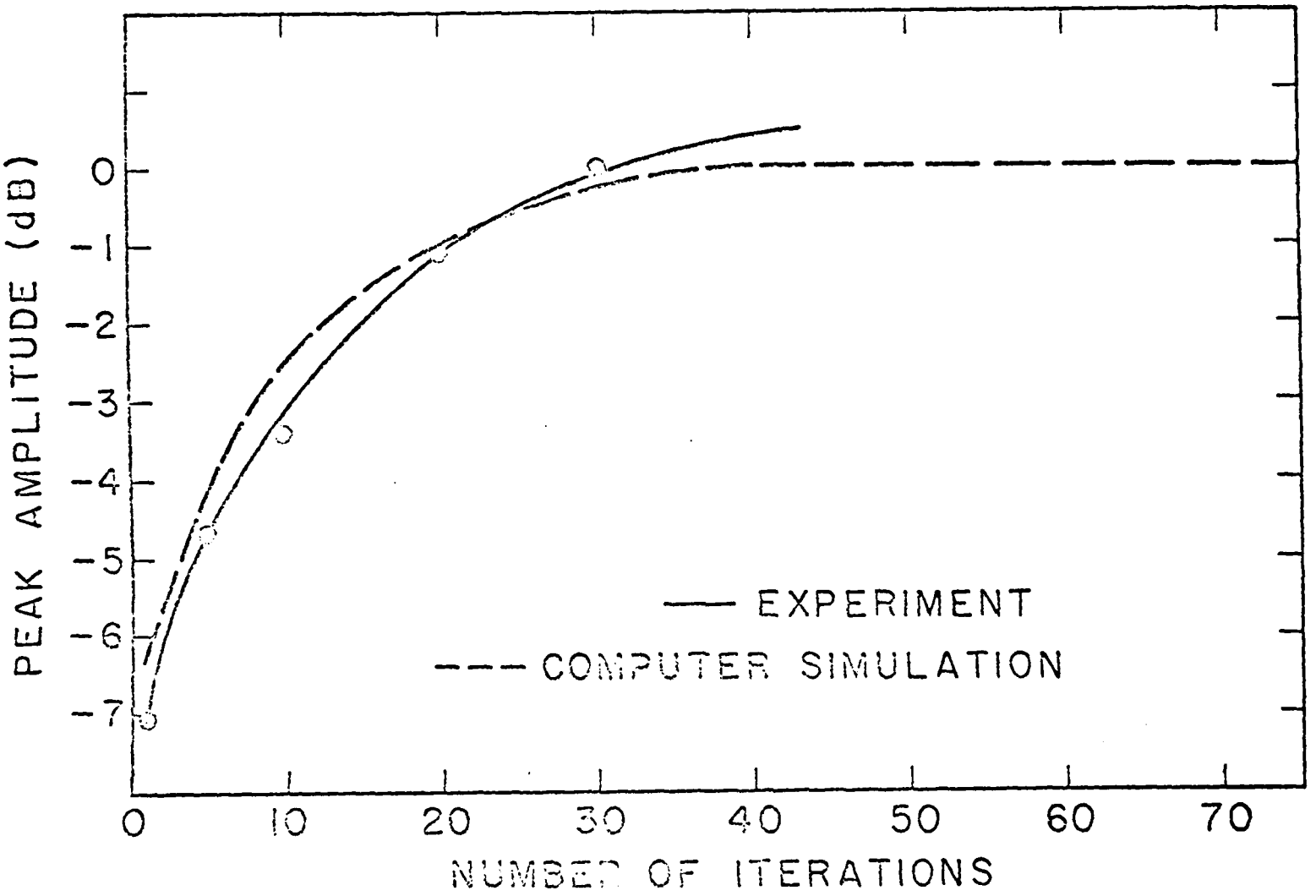
PEAK AMPLITUDE (dB)
0
-1
-2
-3
-4
-5
-6
-7
0
10
20
30
40
50
60
70
NUMBER OF ITERATIONS
EXPERIMENT
COMPUTER SIMULATION

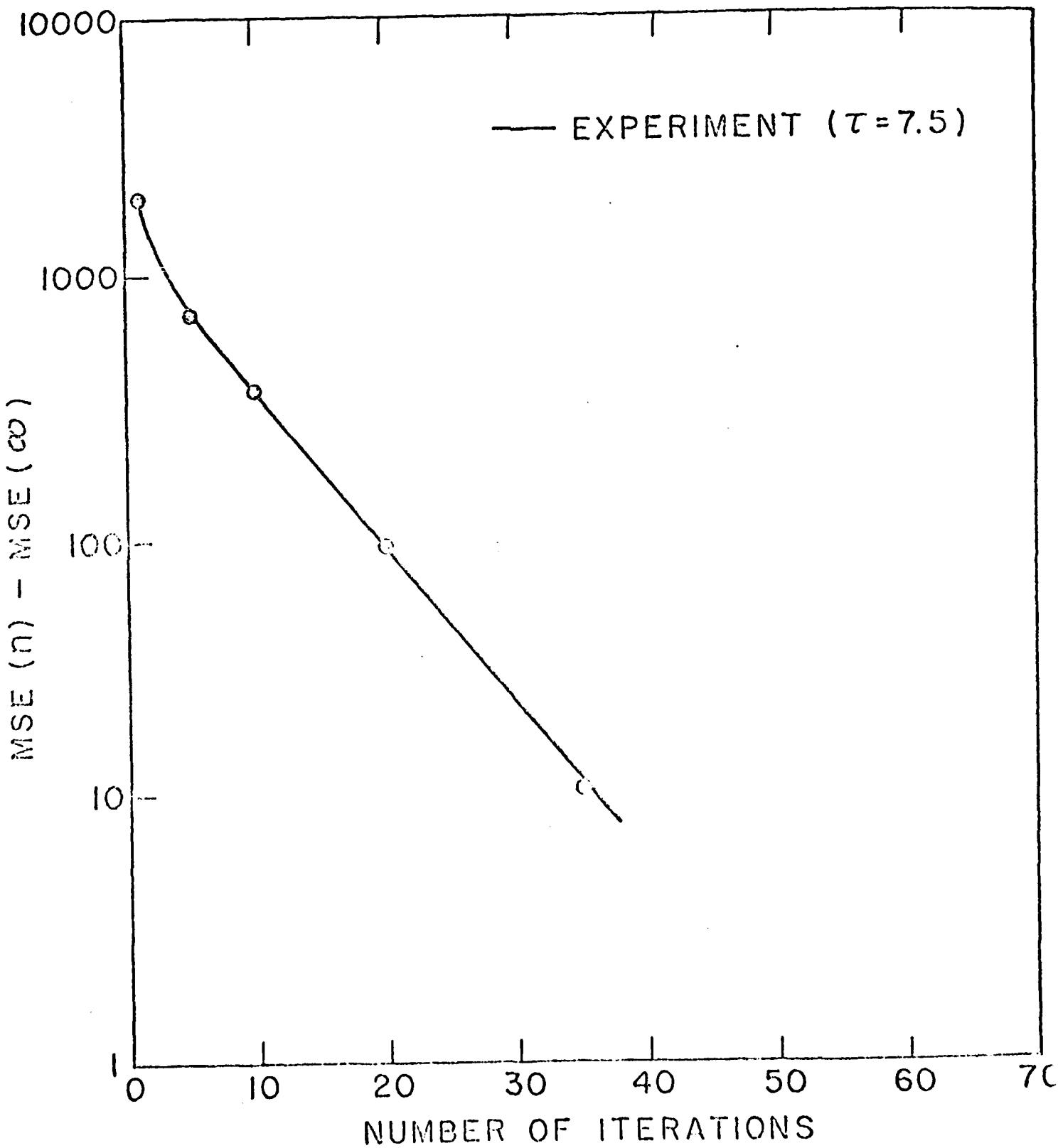
10000
1000
100
10
1
0
10
20
30
40
50
60
70
EXPERIMENT (τ=7.5)
MSE (n) - MSE (∞)
NUMBER OF ITERATIONS